



NAVAL POSTGRADUATE SCHOOL

MONTEREY, CALIFORNIA

THESIS

**DESIGN AND INSTALLATION OF A FIELD IONIZATION
TEST CHAMBER FOR ION THRUSTERS**

by

Paul W. Camp

December 2011

Thesis Co-Advisors:

Sebastian Oswald

Marcello Romano

Second Reader:

Oscar Biblarz

Approved for public release; distribution is unlimited

THIS PAGE INTENTIONALLY LEFT BLANK

| | | | | |
|--|---|--|--|--|
| REPORT DOCUMENTATION PAGE | | | <i>Form Approved OMB No. 0704-0188</i> | |
| Public reporting burden for this collection of information is estimated to average 1 hour per response, including the time for reviewing instruction, searching existing data sources, gathering and maintaining the data needed, and completing and reviewing the collection of information. Send comments regarding this burden estimate or any other aspect of this collection of information, including suggestions for reducing this burden, to Washington headquarters Services, Directorate for Information Operations and Reports, 1215 Jefferson Davis Highway, Suite 1204, Arlington, VA 22202-4302, and to the Office of Management and Budget, Paperwork Reduction Project (0704-0188) Washington DC 20503. | | | | |
| 1. AGENCY USE ONLY (Leave blank) | | 2. REPORT DATE December 2011 | 3. REPORT TYPE AND DATES COVERED Master's Thesis | |
| 4. TITLE AND SUBTITLE Design and Installation of a Field Ionization Test Chamber for Ion Thrusters | | | 5. FUNDING NUMBERS | |
| 6. AUTHOR(S) LT Paul W. L. Camp | | | | |
| 7. PERFORMING ORGANIZATION NAME(S) AND ADDRESS(ES) Naval Postgraduate School Monterey, CA 93943-5000 | | | 8. PERFORMING ORGANIZATION REPORT NUMBER | |
| 9. SPONSORING /MONITORING AGENCY NAME(S) AND ADDRESS(ES) N/A | | | 10. SPONSORING/MONITORING AGENCY REPORT NUMBER | |
| 11. SUPPLEMENTARY NOTES The views expressed in this thesis are those of the author and do not reflect the official policy or position of the Department of Defense or the U.S. Government. IRB Protocol number _N/A_. | | | | |
| 12a. DISTRIBUTION / AVAILABILITY STATEMENT Approved for public release; distribution is unlimited | | | 12b. DISTRIBUTION CODE A | |
| 13. ABSTRACT (maximum 200 words) <p>The utilization of carbon nanotube arrays for field ionization in ion thrusters allows for a substantial reduction in thruster size and weight. The availability of miniature ion thrusters may enable the development of a suitable propulsion system for nano- and picosatellites, and can realize substantial weight, volume, and cost savings in existing satellite platforms.</p> <p>This research focuses on the design of a field ionization test chamber that can be used to determine a comprehensive performance metric for the carbon nanotube field ionization micro-ion thruster (CNT-FIMIT). Using the knowledge gathered from two previously employed test chamber designs, a third generation apparatus with higher precision and improved capabilities is constructed. This new design incorporates a mass flow controller for propellant flow rate measurements, a high-voltage source-measure unit for ionization current measurements, and a linear shift with position feedback for adjusting the distance between the carbon nanotubes and the counter electrode during field-ionization. The design emphasizes user-friendly operation by simplifying the sample exchange and by reducing the chamber volume under vacuum for a faster turn-around time between experiments. The proposed design is highly modular, allowing for easy installation of additional analytic capabilities and other future upgrades.</p> | | | | |
| 14. SUBJECT TERMS carbon nanotube, ion thruster, nanosatellite, test chamber | | | 15. NUMBER OF PAGES 93 | |
| | | | 16. PRICE CODE | |
| 17. SECURITY CLASSIFICATION OF REPORT Unclassified | 18. SECURITY CLASSIFICATION OF THIS PAGE Unclassified | 19. SECURITY CLASSIFICATION OF ABSTRACT Unclassified | 20. LIMITATION OF ABSTRACT UU | |

NSN 7540-01-280-5500

Standard Form 298 (Rev. 8-98)
Prescribed by ANSI Std. Z39.18

THIS PAGE INTENTIONALLY LEFT BLANK

Approved for public release; distribution is unlimited

**DESIGN AND INSTALLATION OF A FIELD IONIZATION TEST CHAMBER
FOR ION THRUSTERS**

Paul W. Camp
Lieutenant, United States Navy
B.S., United States Naval Academy, 2003

Submitted in partial fulfillment of the requirements for the degree of

MASTER OF SCIENCE IN ASTRONAUTICAL ENGINEERING

from the

**NAVAL POSTGRADUATE SCHOOL
December 2011**

Author: Paul W. Camp

Approved by: Sebastian Osswald
Thesis Advisor

Marcello Romano
Thesis Co-Advisor

Oscar Biblarz
Second Reader

Knox T. Millsaps
Chair, Department of Mechanical and Aerospace
Engineering

THIS PAGE INTENTIONALLY LEFT BLANK

ABSTRACT

The utilization of carbon nanotube arrays for field ionization in ion thrusters allows for a substantial reduction in thruster size and weight. The availability of miniature ion thrusters may enable the development of a suitable propulsion system for nano- and picosatellites, and can realize substantial weight, volume, and cost savings in existing satellite platforms.

This research focuses on the design of a field ionization test chamber that can be used to determine a comprehensive performance metric for the carbon nanotube field ionization micro-ion thruster (CNT-FIMIT). Using the knowledge gathered from two previously employed test chamber designs, a third generation apparatus with higher precision and improved capabilities is constructed. This new design incorporates a mass flow controller for propellant flow rate measurements, a high-voltage source-measure unit for ionization current measurements, and a linear shift with position feedback for adjusting the distance between the carbon nanotubes and the counter electrode during field-ionization. The design emphasizes user-friendly operation by simplifying the sample exchange and by reducing the chamber volume under vacuum for a faster turn-around time between experiments. The proposed design is highly modular, allowing for easy installation of additional analytic capabilities and other future upgrades.

THIS PAGE INTENTIONALLY LEFT BLANK

TABLE OF CONTENTS

| | | |
|------|---|-----------|
| I. | INTRODUCTION..... | 1 |
| A. | ION THRUSTERS | 1 |
| 1. | Theory of Operation | 1 |
| 2. | Ion Thruster Design | 4 |
| 3. | Ionization Methods | 4 |
| 4. | Current Design Limitations..... | 6 |
| B. | FIELD EMISSION AND FIELD IONIZATION..... | 7 |
| 1. | Field Emission | 7 |
| 2. | Field Ionization..... | 10 |
| C. | CARBON NANOTUBES | 12 |
| 1. | Structure..... | 13 |
| 2. | Properties | 13 |
| 3. | Field Emission Applications | 14 |
| 4. | Field Ionization Applications | 17 |
| D. | CARBON NANOTUBE BASED ION THRUSTERS..... | 17 |
| E. | FIELD IONIZATION TEST CHAMBER | 20 |
| 1. | Generation 1 | 20 |
| 2. | Generation 2..... | 21 |
| 3. | Limitations of Current Designs | 23 |
| a. | <i>Comparison of Continuum and Free Molecular Flow.....</i> | <i>25</i> |
| II. | OBJECTIVES | 27 |
| III. | RESULTS AND DISCUSSION | 29 |
| A. | DESIGN OF THE NEW TEST CHAMBER..... | 29 |
| 1. | Improvements to GEN1 and GEN2 | 29 |
| 2. | Generation 3 Test Chamber | 30 |
| a. | <i>Linear Shift Mechanism with Linear Potentiometer (LSM38–50-SS-LP-UP, Kurt J. Lesker Company)</i> | <i>34</i> |
| b. | <i>Electrode Mount.....</i> | <i>36</i> |
| c. | <i>Sacrificial Mount</i> | <i>36</i> |
| d. | <i>Accelerator Grid Electrode Mount – “Top Hat”</i> | <i>37</i> |
| e. | <i>Sample Electrode Mount</i> | <i>38</i> |
| f. | <i>Thermal Mass Flow Controller (C100, Sierra Instruments)</i> | <i>40</i> |
| g. | <i>High-Voltage Source-Measure Unit (Keithley 237)...</i> | <i>41</i> |
| h. | <i>Complete Test Stand</i> | <i>42</i> |
| B. | FIELD EMISSION AND FIELD IONIZATION TESTING | 46 |
| 1. | Field Emission Testing..... | 46 |
| 2. | Field Ionization Testing..... | 47 |
| IV. | CONCLUSIONS AND OUTLOOK | 49 |
| A. | CONCLUSIONS | 49 |

| | | |
|-------------|---|----|
| B. | OUTLOOK | 50 |
| 1. | Multi-Hole Electrode Mount | 50 |
| 2. | Non-Conductive Electrode Mount for Accelerator Grid | 51 |
| 3. | Mass Flow Meter Downstream of Ionization Chamber | 51 |
| 4. | Downstream Gas Input for Altitude Variation | 52 |
| 5. | Jog Box for Sample Changes | 52 |
| 6. | Replace Upstream Bellows with 100mm Travel Bellows ... | 53 |
| 7. | Linear Encoder for Position Feedback | 53 |
| APPENDIX A. | MECHANICAL DRAWINGS..... | 55 |
| APPENDIX B. | MASS FLOW CONTROLLER OPERATING PROCEDURES. | 59 |
| APPENDIX C. | HIGH-VOLTAGE SOURCE-MEASURE UNIT OPERATING PROCEDURES..... | 63 |
| APPENDIX D. | APPARATUS PARTS LIST..... | 69 |
| | LIST OF REFERENCES..... | 71 |
| | INITIAL DISTRIBUTION LIST | 75 |

LIST OF FIGURES

| | | |
|-----------|--|----|
| Figure 1 | Power requirements for spacecraft propulsion (From [4])..... | 2 |
| Figure 2 | NSTAR electrostatic ion thruster used on Deep Space 1 (From [5]) | 3 |
| Figure 3 | Schematic of electron bombardment ion thruster (From [4]) | 5 |
| Figure 4 | Schematic of FEEP thruster (From [8])..... | 5 |
| Figure 5 | Hall effect thruster (From [4])..... | 6 |
| Figure 6 | Comparison of Hall effect (left) and electron bombardment (middle, right) chamber sizes (from [11])..... | 7 |
| Figure 7 | Potential energy of an electron near the surface of a metal (After [13]) | 8 |
| Figure 8 | Trajectory of gas molecule passing by field ionization tip (From [16]) | 10 |
| Figure 9 | Single-wall (left) and multi-wall (right) CNTs (From [18,19]) | 13 |
| Figure 10 | Tri-grid <i>Inverse Majority Gate</i> design (From [26]) | 15 |
| Figure 11 | Cross Sections of a CRT and FED (From [25]) | 15 |
| Figure 12 | X-ray tube with thermionic source (From [25])..... | 16 |
| Figure 13 | (a) 5 X 10 pixel cathode chip; (b) Structure of CNT cathode; (c) Scanning electron microscope (SEM) image of CNTs (From [27])..... | 17 |
| Figure 14 | Cold cathode for spacecraft applications using CNTs (From [31]) | 19 |
| Figure 15 | CNT-Based ion thruster (From [28]) | 19 |
| Figure 16 | Generation 1 FE/FI test chamber (From [19])..... | 20 |
| Figure 17 | Generation 2 FE/FI test chamber (After [28]) | 21 |
| Figure 18 | GEN2 electrode setup (After [28]) | 22 |
| Figure 19 | Affixing the test base to the GEN2 chamber (After [28])..... | 24 |
| Figure 20 | Velocity profile (From [32]) | 26 |
| Figure 21 | GEN3 ionization chamber..... | 31 |
| Figure 22 | Downstream connection of gap adjuster for GEN3 apparatus..... | 31 |
| Figure 23 | GEN3 sample mount option | 32 |
| Figure 24 | GEN3 gap distance determination..... | 33 |
| Figure 25 | Linear shift mechanism with linear potentiometer..... | 35 |
| Figure 26 | Electrode mount | 36 |
| Figure 27 | Sacrificial mount | 37 |
| Figure 28 | Top hat | 38 |
| Figure 29 | Top hat with sacrificial mount and electrode mount attached | 38 |
| Figure 30 | Sample electrode mount..... | 39 |
| Figure 31 | Sample mount with sacrificial mount and electrode mount attached .. | 39 |
| Figure 32 | Thermal mass flow controller (left) with pilot module (right)..... | 40 |
| Figure 33 | MFC mass flow rate determination (From [34]) | 41 |
| Figure 34 | Keithley 237 high-voltage source-measure unit..... | 41 |
| Figure 35 | Complete GEN3 test stand (HVSMU not pictured) | 42 |
| Figure 36 | Sample electrode mount and accelerator grid electrode mount within ionization chamber (LSM bellows suppressed to allow for viewing of mounts)..... | 43 |
| Figure 37 | Sample exchange..... | 44 |

| | | |
|-----------|--|----|
| Figure 38 | Seven-hole electrode mount..... | 51 |
| Figure 39 | McLennan JC100 Jog Box | 52 |
| Figure 40 | Electrode mount | 55 |
| Figure 41 | Sacrificial mount | 56 |
| Figure 42 | Sample mount | 57 |
| Figure 43 | Top hat mount | 58 |
| Figure 44 | Pilot module buttons (From [34]) | 60 |
| Figure 45 | MFC parameters/specifications (located on back of MFC) | 62 |
| Figure 46 | GPIB configuration utility | 64 |
| Figure 47 | LabView GUI for HVSMU | 66 |

LIST OF TABLES

| | | |
|----------|--|----|
| Table 1. | Apparatus parts list..... | 69 |
| Table 2. | Apparatus parts list (continued) | 70 |

THIS PAGE INTENTIONALLY LEFT BLANK

LIST OF ACRONYMS AND ABBREVIATIONS

| | |
|-------|---|
| CNT | Carbon Nanotube |
| CRT | Cathode Ray Tube |
| CFE | Cold Field Emitter |
| FE | Field Emission |
| FED | Field Emission Display |
| FEEP | Field Emission Electric Propulsion |
| FI | Field Ionization |
| GEN1 | Generation 1 |
| GEN2 | Generation 2 |
| GEN3 | Generation 3 |
| GUI | Graphical User Interface |
| HVSMU | High-Voltage Source-Measure Unit |
| IT | Ion Thruster |
| Kn | Knudsen number |
| LP | Linear Potentiometer |
| LSM | Linear Shift Mechanism |
| MFC | Mass Flow Controller |
| MFM | Mass Flow Meter |
| MS | Mass Spectrometry |
| MWNT | Multi-Walled Carbon Nanotube |
| MUF | Mass Utilization Factor |
| NASA | National Aeronautics and Space Administration |
| NPS | Naval Postgraduate School |

| | |
|------|----------------------------------|
| RT | Radiotherapy |
| RTD | Resistance Temperature Detector |
| SEM | Scanning Electron Microscope |
| SWNT | Single-Walled Carbon Nanotube |
| TE | Thermionic Emission |
| TEM | Transmission Electron Microscope |

ACKNOWLEDGMENTS

The pursuit of this thesis has been the most difficult and trying challenge of my military career. Through it all, I have had the esteemed privilege of working with great faculty, and great peers. This will certainly be an experience I will never forget.

Let me first start by thanking the most important participants of this quest. To my fiancée, Lisa. No matter how difficult the task, nor how straining the day, you were there, cheering me on to the very end. I am forever thankful to be at the end of this long road with you at my side. To my father, mother, and brother. Thank you for your never-ending support and enthusiasm towards this goal. This would not have been possible without the support of each one of you.

I would next like to thank my advisor, Professor Sebastian Osswald, for his guidance and zeal throughout this endeavor. It has been an absolute pleasure working on this project, and I look forward to raising a glass with you in its success. I would also like to thank Professor Oscar Biblarz, for his wealth of knowledge on ion propulsion he imparted to me.

A special thank you goes to Bryan Shrank for allowing me the opportunity to work by his side on his thesis. The experience of working with your apparatus was paramount. Also to Jay Adeff, whose ideas laid the groundwork for designing this test chamber.

Much appreciation goes to both George Jaksha and Dan Sakoda. The components you produced were of the highest quality, and made possible the completion of this test chamber.

Lastly, to all who have ever looked up at the stars and wondered if we could ever reach them. This research, this technology, may very well be your answer. To those who want to take the next step, the opportunity is yours. To those who want to see it happen for yourself, I invite you to come and watch.

THIS PAGE INTENTIONALLY LEFT BLANK

I. INTRODUCTION

A. ION THRUSTERS

Ion thrusters (ITs) constitute a form of electric propulsion utilized for spacecraft propulsion. This form of propulsion, also known as electrostatic propulsion, utilizes Coulomb forces to accelerate ions in the direction of an applied electric field. Overall, they allow for much higher specific impulses¹, as compared to chemical propulsion, and utilize significantly less mass. The generated thrust, however, is significantly less than that obtained from chemical propulsion. These facts make ITs perfectly suited for spacecraft applications. The limiting factors are the size of these thrusters, and the large power requirements necessary to operate them. A typical nanosatellite has a mass range of 1–10kg [1]. In comparison, the National Aeronautics and Space Administration (NASA) Solar Electric Propulsion Technology Application Readiness (NSTAR) electrostatic ion thruster, used on the Deep Space 1 spacecraft, has a mass of 8.3kg [2]. Power requirements for electrostatic thrusters (Hall effect and ion thrusters) can range from 1–10kW (Figure 1). Due to their size restrictions, nanosatellites are unable to produce such high power levels. A potential utilization of ITs aboard nano- and picosatellite platforms therefore requires a new approach to thruster design that lowers power and mass requirements, and allows for substantial reduction in IT size.

1. Theory of Operation

Similar to chemical propulsion, electrostatic propulsion accelerates spacecraft through the principle of conservation of momentum. However, instead of accelerating the propellant by differential pressures or through combustion, electrostatic propulsion utilizes Coulomb forces to accelerate the propellant.

¹ Specific Impulse (I_s) is defined as the total impulse per unit weight of propellant. It is calculated by: $I_s = F / (\dot{m} \cdot g_o)$, where F is thrust, \dot{m} is the mass flow rate of the propellant, and g_o is the standard acceleration due to gravity at sea level [1]. It provides a measure of performance between different propulsion systems.

According to Coulomb's law, the magnitude of the electrostatic forces between two point charges is directly proportional to the product of the charges, and inversely proportional to the square of their distance [3]. If point charges are of the same sign, they will repel each other; if they are of opposite signs, they will attract. It also follows that both electrons and ions can be used for propulsion. However, since the mass of an ion is orders of magnitude greater than the mass of an electron, unipolar ions are used as they provide significantly greater momentum to impart on the spacecraft.

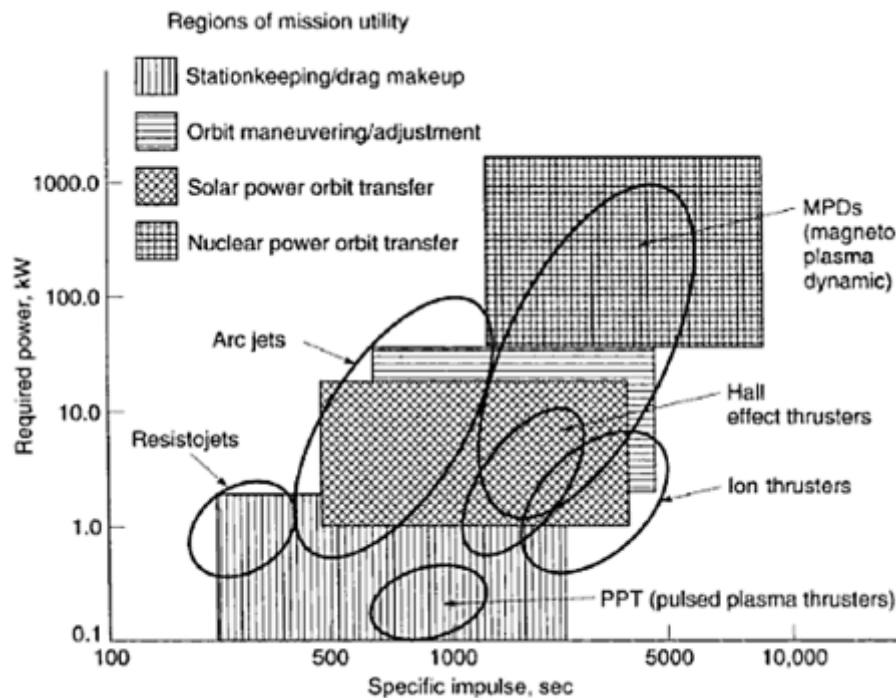


Figure 1 Power requirements for spacecraft propulsion (From [4])

Figure 2 shows an illustration of the NSTAR IT used on the Deep Space 1 spacecraft. Propellant is ionized by means of electron bombardment. A heated cathode at the entrance of the ionization chamber supplies electrons. These electrons are guided by magnetic fields to impact the propellant, causing it to ionize. All electrons (including those newly formed and those used for bombarding the propellant) are attracted to the positively charged grid electrode

(anode), where they are collected. To take advantage of Coulomb's Law, this thruster uses grid electrodes at different electric potentials to accelerate the ions [4].

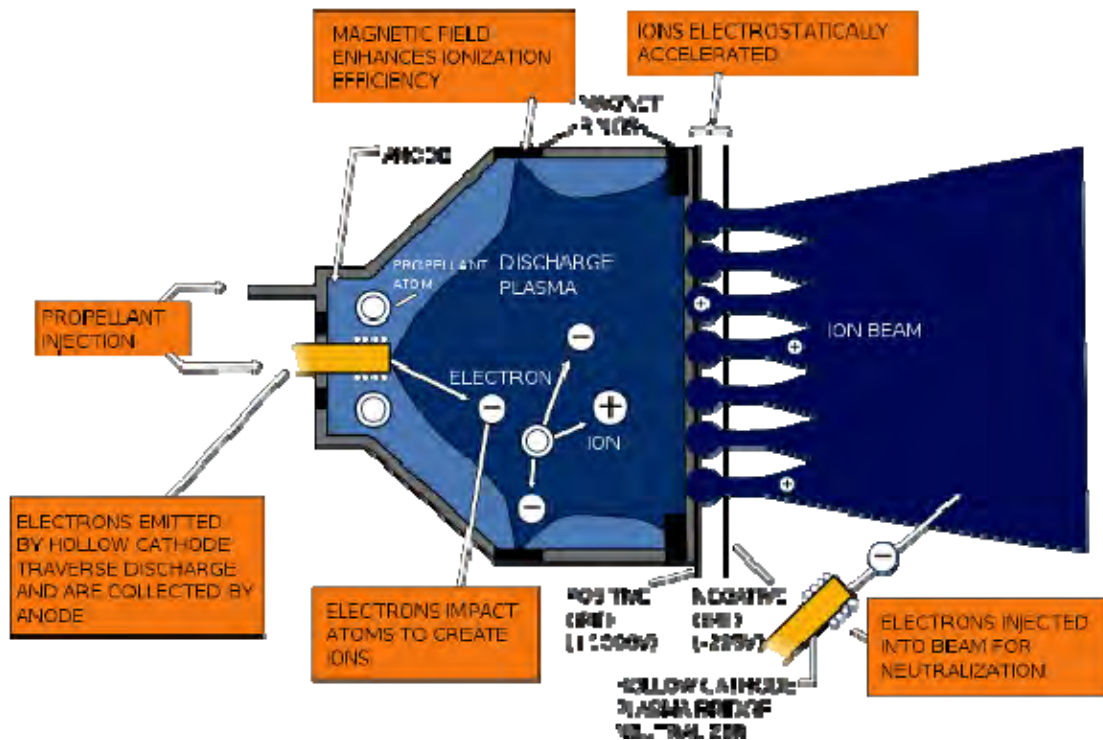


Figure 2 NSTAR electrostatic ion thruster used on Deep Space 1 (From [5])

The grid electrodes are of opposite signs to generate an electric field. The first grid electrode (positive) will repel the newly formed positive ions, while the “downstream” grid electrode(s) will attract it. This will accelerate the ions out of the thruster, and thus, by conservation of momentum, accelerate the spacecraft in the opposite direction. To prevent charging of the spacecraft from the positively charged ion beam exhaust, the IT will have an electron emitter outside of the thruster that will supply electrons to neutralize the ions [6].

2. Ion Thruster Design

The primary components of electrostatic thrusters are a propellant source, several forms of electric power, an ionizing chamber, an accelerator region, and a means of neutralizing the exhaust. The propellant source provides the ions. These are obtained by either ionizing a gas, or by “extracting” ions from a liquid metal. The electric power sources provide the voltages to create the electric field to accelerate the ions, as well as to power other required components of the thruster (i.e., for electrical heating of cathodes to provide electrons for ionization and/or exhaust beam neutralization, and to power magnetic field generators to contain electron paths for ionization). The ionization chamber generates the ions. The accelerator region contains the means by which to accelerate the ions (i.e., using grid electrodes or a negatively charged electron cloud). A neutralizer is used to neutralize the positively charged exhaust beam so the ions cannot return to the spacecraft and cause electrostatic damage or corrosion [4].

3. Ionization Methods

Ionization occurs in ITs by one of the following methods: Electron bombardment, field emission (FE), or Hall effect. For electron bombardment, positive ions are produced by “bombarding” a gas or vapor with electrons usually emitted from a heated cathode [4]. The electrons are accelerated by either the electric field generated between the cathode and anode (DC ionization), or by the oscillating electric field induced by an alternating magnetic field of a coil (RF ionization) [6]. The ions are accelerated by grids with opposing potentials (Figure 3).

In Field Emission Electric Propulsion (FEEP), ions are obtained from a liquid metal source (either Cesium or Indium) flowing through a capillary tube [4]. Once the liquid metal reaches the end of the tube, an electric field applied between the emitter and the accelerator ring ionizes the liquid, causing the surface to deform and emit positive ions [7]. The ions are then accelerated by the same electric field applied between the emitter and the accelerator (Figure 4).

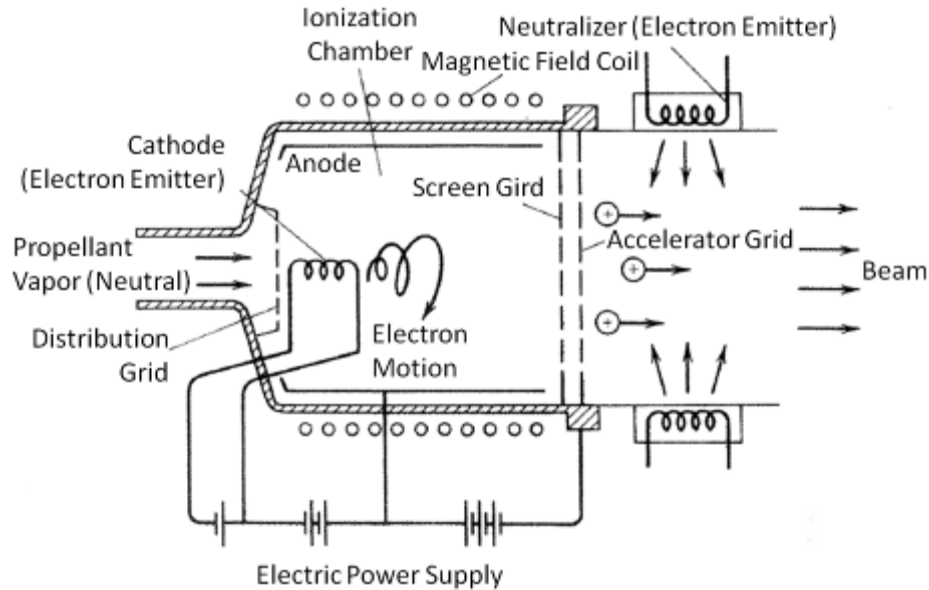


Figure 3 Schematic of electron bombardment ion thruster (From [4])

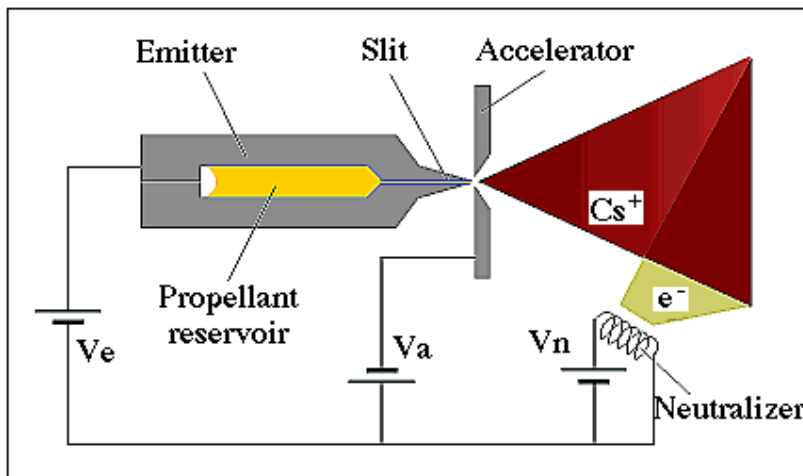


Figure 4 Schematic of FEEP thruster (From [8])

Hall effect thrusters improve upon the concept of electron bombardment. Instead of using grid electrodes to accelerate ions, the Hall effect thruster uses magnets to generate and maintain a negatively charged plasma cloud at the exit of the thruster (Figure 5). This generates the negative potential to accelerate the ions. Collisions with other particles and walls, as well as electrostatic fluctuations, allow some of the electrons to be freed from the magnetic field, causing them to

drift towards the anode [6]. These electrons are used to ionize the propellant. This design is more compact than electron bombardment, but higher in mass because of the more powerful magnets that are required to contain the electron cloud.

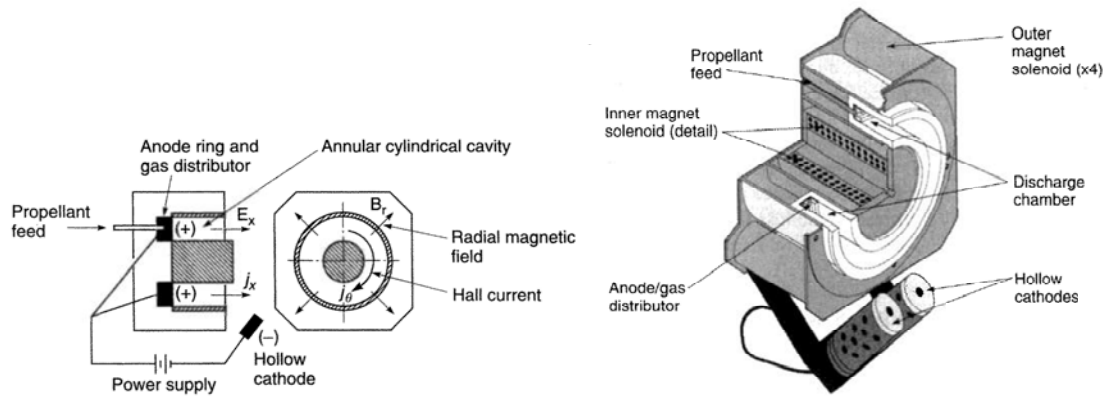


Figure 5 Hall effect thruster (From [4])

4. Current Design Limitations

Current IT designs are impractical for use on nano- and picosatellites. Since the minimum IT chamber size is dictated by the space requirements of the various thruster components needed for ionization (e.g., cathodes, magnets), chamber sizes of current IT technologies are larger than nanosatellites, as a whole² (Figure 6).

As stated above, Hall effect thrusters are smaller in size, as compared to electron bombardment thrusters, but higher in mass because of the magnets needed to contain the negatively charged plasma cloud used as the cathode. The primary factor that constrains reduction in size is the need for magnets. Scaling to low-power requires a decrease in the thruster channel size, and an increase in the magnetic field strength. An increase in the magnetic field can

² A 1U CubeSat has dimensions of 10cm x 10cm x 10cm [9].

result in saturation of the miniaturized inner components of the magnetic circuit, and scaling down the magnetic circuit does not leave enough room for magnetic pole pieces and heat shields [10].

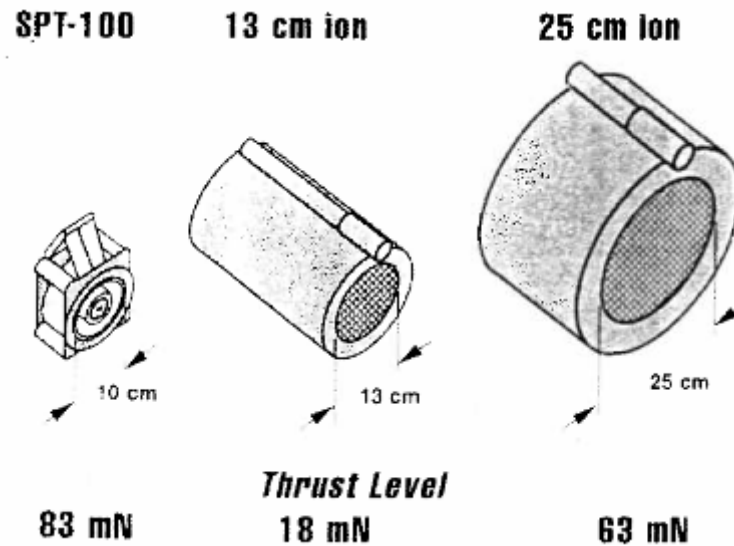


Figure 6 Comparison of Hall effect (left) and electron bombardment (middle, right) chamber sizes (from [11])

In addition to their sizes, the power required to heat the cathodes for electron production, and to power the magnets for electron path containment, far exceed what can be produced by nanosatellites. Thus, reducing the size and power requirement of today's ITs is the goal to using them on nanosatellites.

B. FIELD EMISSION AND FIELD IONIZATION

1. Field Emission

FE is defined as the emission of electrons from the surface of a condensed phase into another phase, usually a vacuum, in the presence of high electrostatic fields [12]. It is accomplished by applying a high enough electric field across a metal surface, resulting in electrons being “pulled” out of the metal.³ The

³ This “pulling” of electrons out of the metal is commonly referred to as “tunneling.”

magnitude of the electric field required for emission depends on the Fermi level (E_f) and the work function (ϕ) of the metal in use.

The Fermi level is the energy region of a metal atom in which free electron theory prevails. In this region, valence electrons form an electron “cloud” and are free to move about the metal’s lattice (Figure 7). This property gives rise to the conductivity of metals, and determines its electrical and thermal properties. Since these electrons have a weak attraction to the nucleus, it is possible to create a state by which the electrons will move out of the lattice. Means by which to emit electrons include photoemission (using light), thermionic emission (TE) (using heat), and FE (using electric fields). The energy required for the electron to escape the pull of the nuclei is known as the work function of the metal.

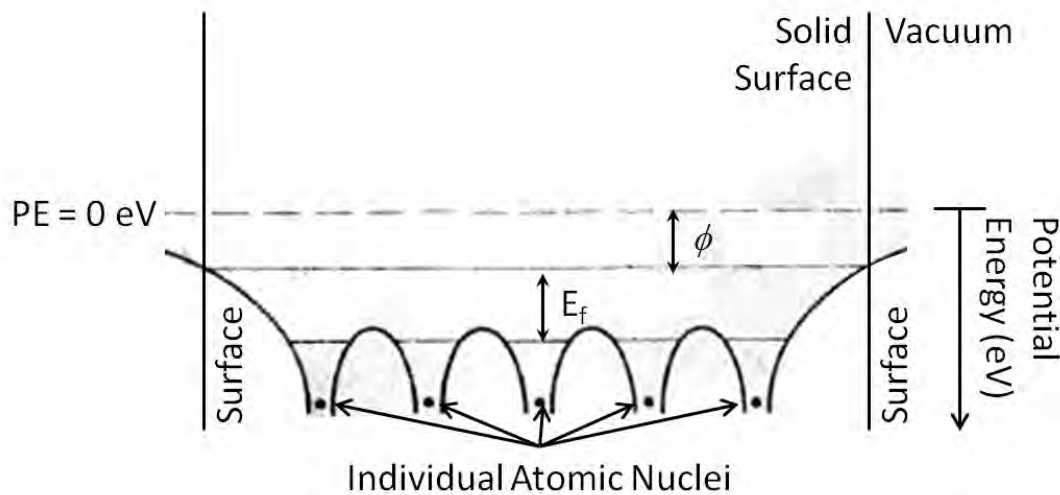


Figure 7 Potential energy of an electron near the surface of a metal (After [13])

In 1928, R.H. Fowler and L. Nordheim developed an expression that described the local current (I) generated from the internal electron states in the conduction band of a bulk metal [14]. This expression is a function of the work function (ϕ) of the metal, and the magnitude of the local field (F) at the emitter:

$$I = \frac{A}{\phi} \cdot F^2 \exp\left(\frac{-B \cdot \phi^{\frac{3}{2}}}{F}\right),$$

Equation 1: Fowler-Nordheim equation for field emission (I-V form)

where A and B are constants, equaling $1.541\text{E-}6 \frac{A \cdot eV}{V^2}$ and $6.831\text{E}9 \frac{V}{eV^{\frac{3}{2}} \cdot m}$, respectively.

By taking the natural logarithm of Equation 1, we obtain:

$$\ln(I) = \left(-B\phi^{\frac{3}{2}}\right)\left(\frac{1}{F}\right) + \ln\left(\frac{A}{\phi}F^2\right).$$

Equation 2: Plottable form of fowler-nordheim equation

Also, the local electric field can be related to the applied voltage (V_a) by:

$$F = \beta \cdot V_a,$$

Equation 3: Geometric field enhancement factor relation

where β represents the geometric field enhancement factor. This value gives a measure of how effectively the needle-tip emitter is amplifying the applied field/voltage, and yields a means to compare various emitter configurations. If the F^2 term is moved to the left side of Equation 1, and Equation 3 is substituted, the new equation is:

$$\ln\left(\frac{I}{V_a^2}\right) = \left(\frac{-B \cdot \phi^{\frac{3}{2}}}{\beta}\right)\left(\frac{1}{V_a}\right) + \ln\left(\frac{A}{\phi \cdot \beta^2}\right).$$

Equation 4: Plottable form of Fowler-Nordheim equation (corrected)

At first, Fowler and Nordheim noted that the plot of $\ln(I)$ vs. $\ln\left(\frac{1}{V_a}\right)$ should yield a straight line whenever the experimental conditions are sufficiently stable [14]. In 1929, however, T.E. Stern, B.S. Gossling, and Fowler determined

that the relation between $\ln\left(\frac{I}{V_a^2}\right)$ and $\left(\frac{1}{V_a}\right)$ should be more accurately linear than the relation between $\ln(I)$ and $\left(\frac{1}{V_a}\right)$ [15]. Using Equation 4, with ϕ known, and I and V_a measured directly, β can be calculated directly from the slope of the plot $\ln\left(\frac{I}{V_a^2}\right)$ vs. $\left(\frac{1}{V_a}\right)$.

In most literature, the β^2 term is omitted. This is acceptable because it only affects the plot by shifting it along the y-axis; it does not affect the slope. Thus, β can be determined accurately without the inclusion of the β^2 term.

2. Field Ionization

Field ionization (FI) is effectively FE in reverse. It involves the tunneling of electrons from an atom into the tip of an ionizer [12]. The two key factors in FI are the magnitude of the applied field and the geometry of the ionizer [12]. Much like work functions in FE, ionization potentials define the energy level required to pull electrons out of gas molecules. The geometry of the ionizer impacts to what degree the local field is enhanced. This enhancement is known as the geometric enhancement factor, defined in Equation 3. According to Equation 3, the sharper the tip of the ionizer, the greater the increase in the local electric field. Figure 8 illustrates the impact an ionizer has on a gas molecule.

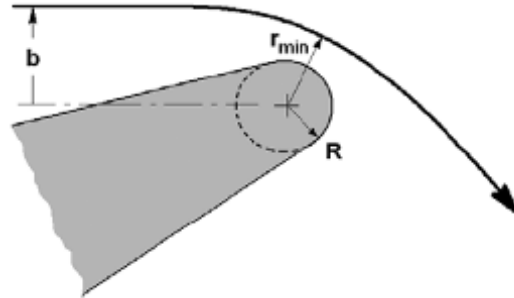


Figure 8 Trajectory of gas molecule passing by field ionization tip (From [16])

For this illustration, the ionizer tip is modeled as a sphere with radius R . The impact parameter b represents the initial energy state, with respect to the ionizer. r_{min} is the closest point of approach for the molecule. There is a critical value b^* , such that, if $b > b^*$, the molecule will not be ionized:

$$b^* = \left(\frac{2 \cdot \alpha \cdot V_0^2 \cdot R^2}{E_0} \right)$$

Equation 5: Critical impact parameter (From [16])

Equation 5 shows that the potential, V_0 , is inversely proportional to the size of the ionizer. Thus, the sharper/smaller the ionizer, the greater the local electric field at the tip.

A means of measuring the performance of the ionizer is by measuring the current generated by the ionized gas ($I_{measured}$), and comparing this number to the maximum theoretical current that should be generated. The maximum theoretical ion current is calculated using Equation 6:

$$I_{max} = \dot{m} \left(\frac{e}{\mu} \right),$$

Equation 6: Maximum theoretical current of field ionizer (From [4])

where \dot{m} is the mass flow rate of the propellant through the ionizer, e is the electrical charge of the singly ionized mass (1.602E-19 C), and μ is the mass of the charged particle (molecular mass of the particle times the mass of a proton, 1.673E-27 kg). This equation assumes all of the propellant passing through the ionizer is singly charged. The ratio of $I_{measured}$ to I_{max} yields a mass utilization factor (MUF) for the ionizer, which is the percentage of the propellant being ionized.

I_{max} can also be used to calculate the ideal thrust of an IT (Equation 7):

$$F = I_{\max} \sqrt{\frac{2 \cdot \mu \cdot V_{acc}}{e}},$$

Equation 7: Ideal thrust of IT (From [4])

where V_{acc} is the voltage across the grid electrodes used to accelerate the ions (i.e., the applied voltage). The ideal thrust can also be calculated using Equation 8:

$$F = B \cdot V_{acc}^2 \left(\frac{D}{d} \right)^2,$$

Equation 8: Alternate calculation of ideal thrust of IT (From [4])

where B equals $\left(\frac{2}{9} \right) \pi \epsilon_o$, or $6.18\text{E-}12 \frac{C}{V \cdot m}$, D is the exhaust beam emitter diameter, and d is the electrode grid spacing, or gap distance. An expression for $I_{\max}(V_{acc}, D, d)$ can be made by equating Equation 7 and Equation 8:

$$I_{\max} = B \cdot \left(\frac{D}{d} \right)^2 \sqrt{\frac{V_{acc} \cdot e}{2 \cdot \mu}}$$

Equation 9: Maximum theoretical current as a function of applied voltage, electrode gap distance, and exhaust beam emitter diameter

Equation 9 shows that the maximum theoretical current is inversely proportional to the electrode gap distance.

C. CARBON NANOTUBES

The material requirements for effective field emitters and field ionizers are high strength, high thermal conductivity, and high electrical conductivity. Carbon Nanotubes (CNTs) display all of these properties. In addition, their extremely small sizes allow for miniaturization of current FE and FI applications. These characteristics make CNTs an ideal candidate for use as field emitters and field ionizers for spacecraft propulsion.

1. Structure

CNTs can be pictured as cylindrical, hollow tubes made up of one-atom-thick sheets of carbon, called graphene. CNTs are generally characterized into single-wall CNT (SWCNT), which consist of only one graphene wall, and multi-walled CNT (MWCNT), which consist of multiple, concentric walls of graphene (Figure 9). One of the most unique features of CNTs is their extremely high aspect ratio (length-to-diameter ratio). SWCNTs have diameters on the order of one nanometer (nm), but reach lengths up to the centimeter range, giving it aspect ratios of up to 10^{11} [17].

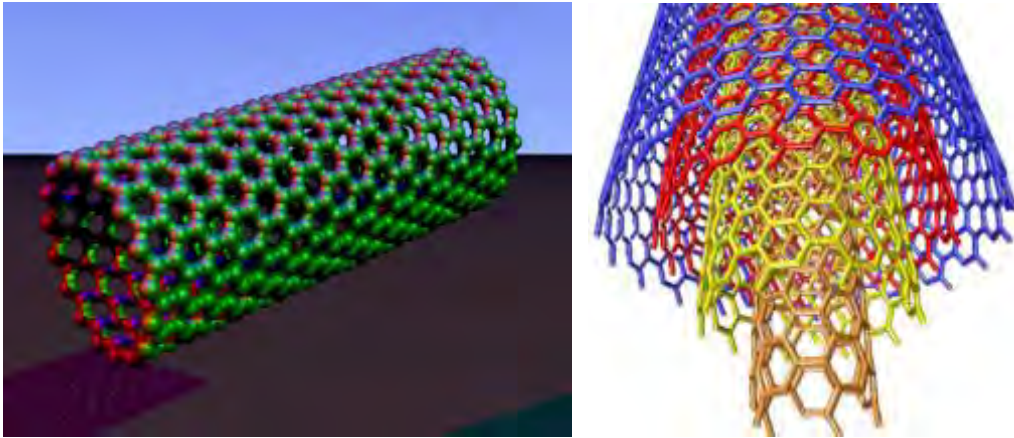


Figure 9 Single-wall (left) and multi-wall (right) CNTs (From [18,19])

2. Properties

CNTs have very desirable strength, electrical, and thermal properties. Compared to SAE-1090 carbon steel's ultimate strength of 841 MPa [20], CNTs currently have the highest strength known to man, with an ultimate strength of up to 63,000 MPa [21]. Dependent upon its structure, CNTs can exhibit metallic or semiconducting properties. In theory, metallic CNTs can carry an electric current density of $\sim 4\text{E}9 \frac{\text{A}}{\text{cm}^2}$, which is more than 1000 times greater than that of highly conducting metals, such as copper [22]. CNTs are also great thermal conductors

along their axes, and good insulators along the tube's radius. The theoretical thermal conductivity of SWCNT along the tube's axis is $\sim 3500 \frac{W}{m \cdot K}$ [23]; compare this to copper, a metal well known for its good thermal conductivity, which transmits $401 \frac{W}{m \cdot K}$ [24].

3. Field Emission Applications

The electrical properties of CNTs make them the perfect choice for FE applications. As stated before, they can generate a very high electric current density with minimal to no heat generation.⁴ Their extremely small size also allows for the possibility of miniaturizing a lot of today's FE applications.

Some of the areas where CNTs are being used as FE sources are vacuum microelectronics, field emission displays (FEDs), and x-ray technology. Vacuum electronics is based on the controlled progression of electrons in a vacuum to obtain a signal gain [25]. An example of this is the classic vacuum tube. Because they do not release heat during emission, and because they can be miniaturized, CNTs can replace the thermionic emitter in vacuum tubes. In another application, NASA's Jet Propulsion Laboratory in Pasadena, California, is currently using CNTs as electron current sources for the actuation of logic gates. Their *Inverse Majority Gate* consists of three gates and an anode (Figure 10). By controlling the electron emission from the CNTs to either the anode, or one, two, or all three gate electrodes, logic operation of a 2-input Negated-AND gate and a 2-input Negated-OR gate can be realized from a single device [26]. Because of their high temperature tolerance, and resistance to radiation, this device is aptly suited to space applications.

Much like cathode ray tube (CRT) displays, FEDs are based on the controlled bombardment of electrons on a phosphor film to locally induce light

⁴ This type of emitter is referred to as a Cold Field Emitter, or CFE.

emission [25].⁵ The difference between CRTs and FEDs is the fact that while a CRT uses a single electron source that scans the display, FEDs use an electron source for each pixel of the display (Figure 11). Brightness is controlled by varying the current on the phosphor element. Since the length of the CNTs can be controlled during growth, they can be placed very close to the phosphor element, resulting in a very thin display.

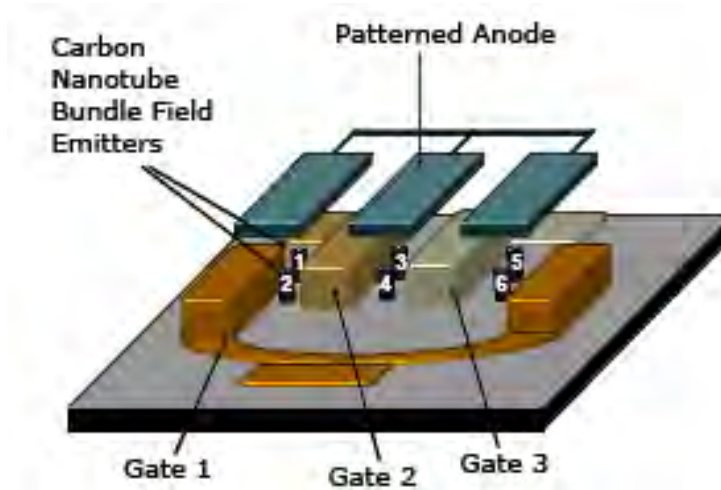


Figure 10 Tri-grid *Inverse Majority Gate* design (From [26])

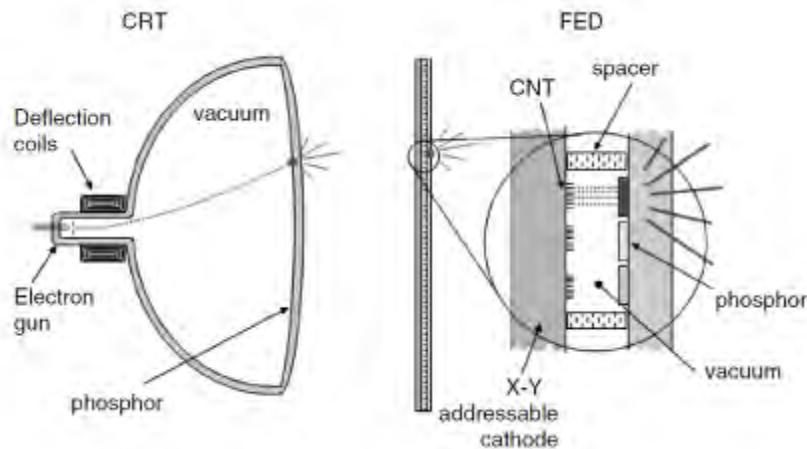


Figure 11 Cross Sections of a CRT and FED (From [25])

⁵ The phosphor converts energy of an incident electron beam into light.

X-ray tubes are the primary components of x-ray source technologies. These tubes allow for the controlled emission of x-rays by bombarding a metallic target with high-energy electrons [25]. The electrons are created through thermal emission (Figure 12). These emitters do not allow for miniaturization due to the generated heat, which reduces their efficiencies below acceptable levels. CNT field emitters can satisfy the needs of miniature x-ray tubes because they do not require heat for the emission of electrons. They also produce high current densities with low applied fields and minimal resistive heating.

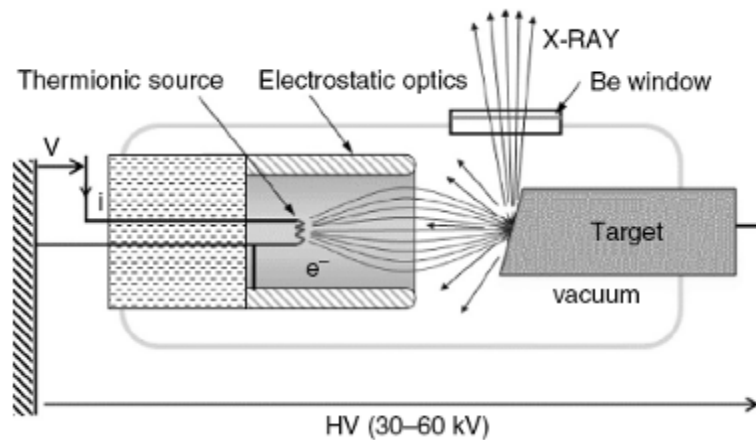


Figure 12 X-ray tube with thermionic source (From [25])

Researchers at the University of North Carolina at Chapel Hill are developing a CNT Field Emission Multipixel X-ray Array Source for microradiotherapy (micro-RT) cancer research (Figure 13). Their goal is to develop a system, based on CNTs, that has high spatial and temporal resolution, that is image-guided, and is capable of delivering radiation treatment similar to human radiotherapy, but at “mouse” scales. Instead of a single radiation source design, their multipixel x-ray tube contains 50 individually controlled CNT cathodes, each producing a pixel x-ray beam via a multipixel x-ray beam array collimator [27]. This design has two key advantages: the source can be turned on/off instantaneously, yielding a temporal resolution on the order of milliseconds, and each pixel can be controlled individually, enabling the micro-RT to vary irradiation patterns and intensity.

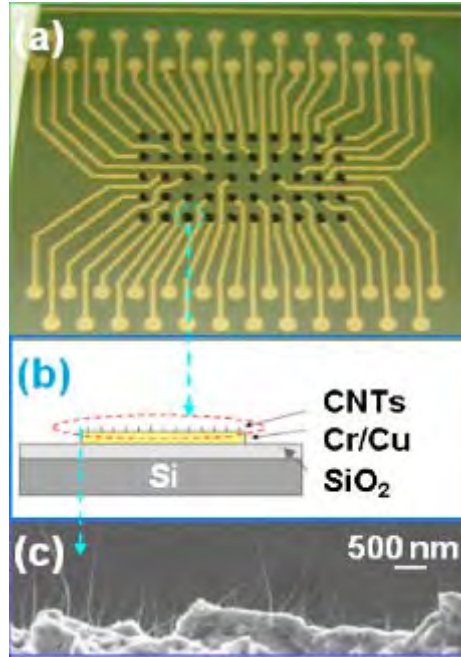


Figure 13 (a) 5 X 10 pixel cathode chip; (b) Structure of CNT cathode; (c) Scanning electron microscope (SEM) image of CNTs (From [27])

4. Field Ionization Applications

The structural array of CNTs is the most important contributor to FI. With diameters as small as nanometers, the tips of CNTs are extremely “sharp.” This results in a significant enhancement of the electric field at the tips of the CNTs (several thousand times) [28].

One application of FI via CNTs is for mass spectrometry (MS). MS measures the mass-to-charge ratio of charged particles [29]. This is accomplished by ionizing a sample/molecule, then measuring its mass-to-charge ratio. From this, the composition of the sample/molecule can be determined, as well as its mass. Uses for MS with CNTs are gas detectors and partial pressure gauges [30].

D. CARBON NANOTUBE BASED ION THRUSTERS

As shown in the previous section, CNTs can be used to miniaturize FE and FI systems and reduce their power requirements. For current IT designs, FE

via CNTs can replace the cathodes used to supply electrons for electron bombardment ionization and to neutralize the exhaust beam. Present cathodes use TE to generate electrons. Certain cathodes require extra propellant mass to be carried on satellites to provide the source of electrons for TE. This mass is not used for generating thrust. Also, these cathodes have high power requirements, and give off waste heat that is not used during TE. These inefficiencies can be improved, if not eliminated, by using FE via CNTs.

CNTs can serve as the source of electrons, eliminating the need for extra propellant. The field enhancement capability of CNTs can reduce power requirements for extracting electrons by decreasing the input voltage required to achieve emission. At the same time, the FE process does not create excessive heat. Thus, CNTs can serve as an excellent replacement for thermionic emitters in spacecraft.

The Georgia Tech Research Corporation has developed a CNT-based FE system for spacecraft propulsion using CNTs (Figure 14) [31]. This design utilizes CNTs grown on a conductive base layer. An insulating layer is then attached to the base layer, with a conductive gate layer attached to the insulating layer. The insulating layer and conductive gate layer are attached so as to allow a gap for the CNTs to emit electrons.⁶ The base and gate layers generate the field necessary to extract electrons. The base layer has a negative potential, while the gate layer has a positive potential. The results of their preliminary experiments show that units can generate current densities of at least $50 \frac{mA}{cm^2}$, with lifetimes exceeding 1500 hours [31].

At present, there is no published data reporting on the use of FI for ITs. A design being investigated at the Naval Postgraduate School (NPS) intends to employ CNTs as field ionizers (Figure 15). For this design, the CNTs will provide the electric fields necessary to ionize the propellant. The extracted electrons will

⁶ The optional base layer is used if additional structural integrity is desired.

tunnel into the CNT tips, which also provide the initial positive potential to accelerate the ions, with the accelerator grids providing the subsequent negative potentials.

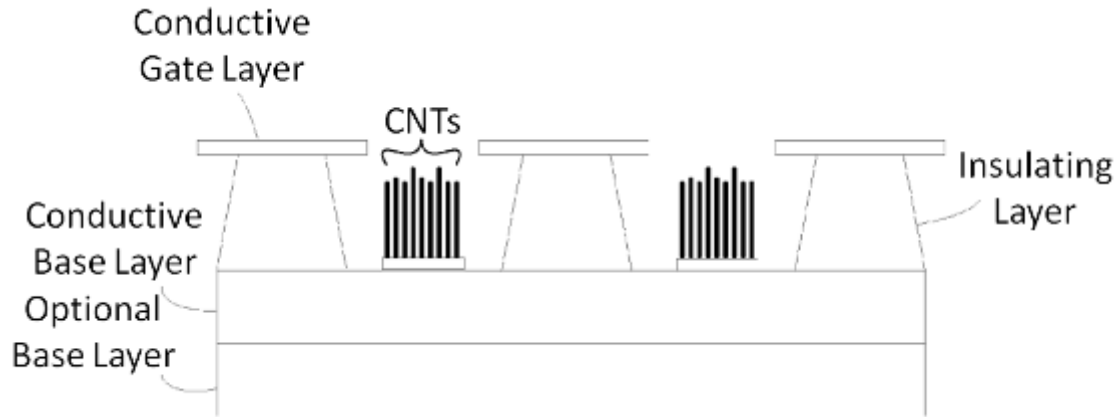


Figure 14 Cold cathode for spacecraft applications using CNTs (From [31])

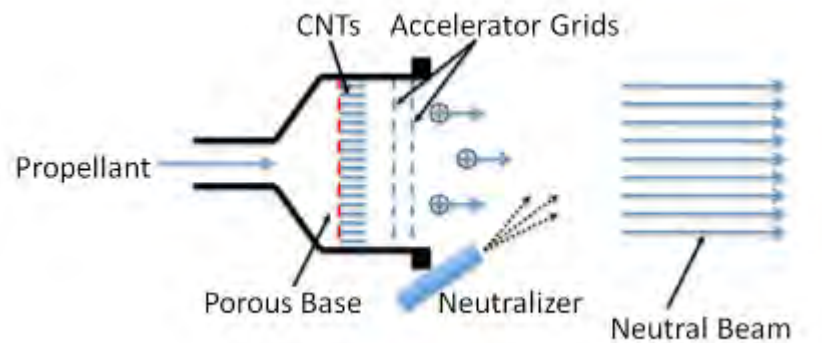


Figure 15 CNT-Based ion thruster (From [28])

The advantages of using CNT-based FI are similar to the benefits discussed in the case of CNT-based FE. The most significant advantages are the elimination of magnets for controlling and containing the electrons, and the ability to drastically reduce the size and weight of the system. This design can make the ionizer depth very compact, compared to Hall and electron bombardment thrusters. For Hall thrusters, the majority of the dry mass comes from the magnets employed, whereas for electron bombardment, the limiting factor is the

size of the ionization chamber needed to host both the cathodes for thermal emission and the magnetic coils. The proposed CNT-field ionization technology is highly complementary to the FE exhaust beam neutralizer developed by researchers at Georgia Tech, and both may be integrated together into a complete CNT-based miniature micro-ion thruster.

E. FIELD IONIZATION TEST CHAMBER

1. Generation 1

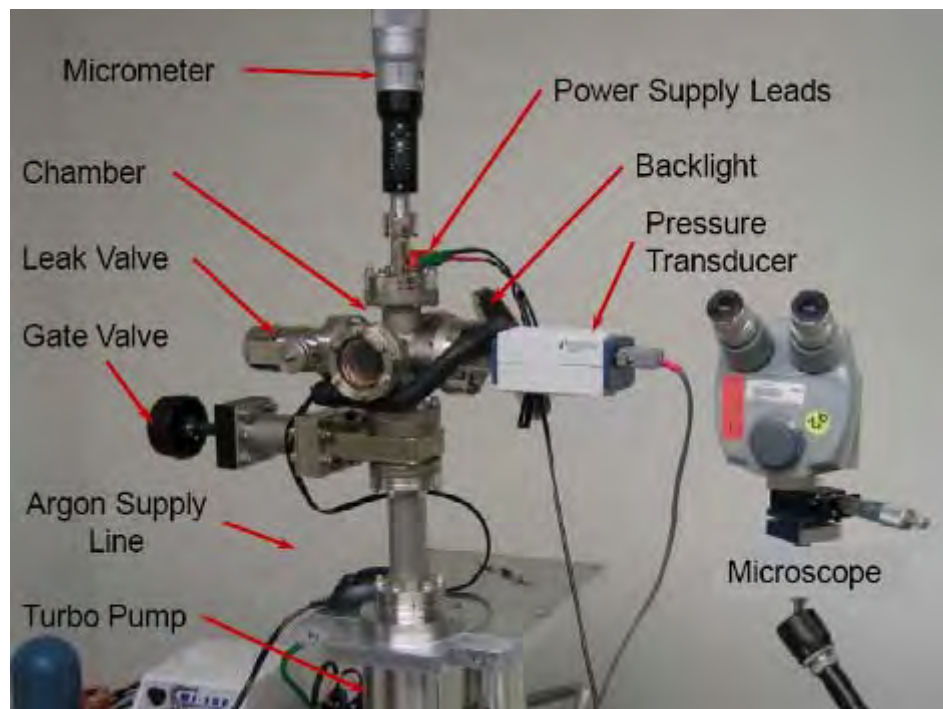


Figure 16 Generation 1 FE/FI test chamber (From [19])

The Generation 1 (GEN1) FE/FI Chamber was designed and used by LT Troy Hicks (USN) during his thesis work at NPS (Figure 16) to test the performance of CNTs he grew at NASA Ames Research Center in California. This apparatus has the basic components needed to measure the performance of CNTs: a vacuum pump, power supply, and gap distance measurement and adjustment. The turbo pump is used to create a pressure differential for the flow of propellant, and to create a vacuum in the test chamber. This vacuum

simulates conditions experienced in space. The power supply provides the voltage put across the electrodes (CNT sample and accelerator grid electrodes). The micrometer adjusts the gap distance between the electrodes.

With this apparatus, LT Hicks confirmed that CNTs correlated with Fowler-Nordheim theory for FE, and measured field enhancement factors as high as 1500. He also measured “turn-on”⁷ applied fields of $5.3 \frac{V}{\mu m}$ and current densities greater than $10 \frac{mA}{cm^2}$ [19].

2. Generation 2

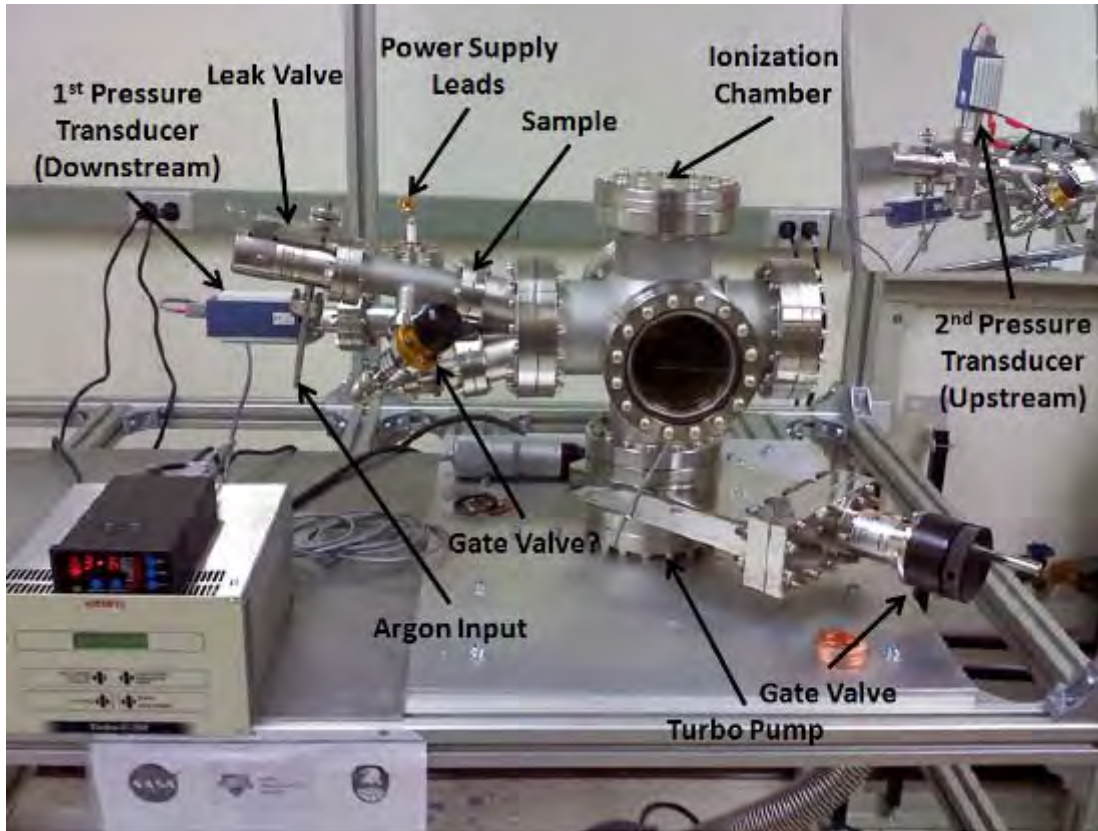
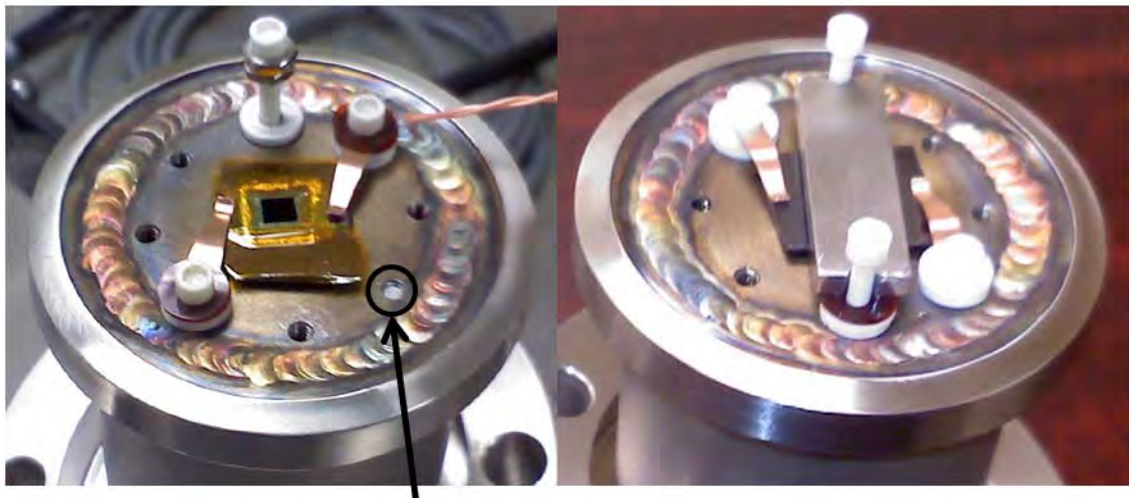
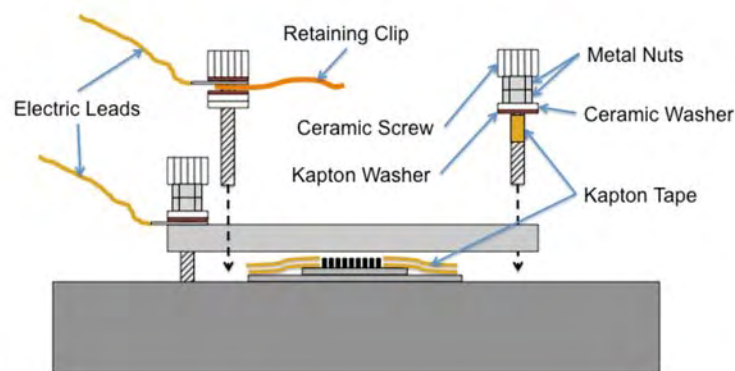


Figure 17 Generation 2 FE/FI test chamber (After [28])

⁷ The “turn-on” field is the point at which CNTs field-emit electrons.

The Generation 2 (GEN2) FE/FI Chamber was designed and used by MAJ Bryan Shrank (USA) during his thesis work at NPS to test the performance of CNTs he grew at NASA Ames (Figure 17). The power leads and vacuum pump serve the same purposes as in the GEN1 design. However, the gap distance between electrodes was set using Kapton tape instead of a micrometer. The gap distance was adjusted by increasing/decreasing the number of layers of Kapton tape. The cathode rested directly on the tape (Figure 18).



Broken Ceramic Screw

Figure 18 GEN2 electrode setup (After [28])

Kapton was also used to electrically isolate the electrodes from each other. MAJ Shrank also determined a mass flow rate calculation for this

apparatus by determining the coefficient of drag of the pre-etched hole⁸ in the sample. From his experiments, MAJ Shrank measured field enhancement factors between 1428 to 5229, and recorded currents around $2.1\text{E-}5$ A, with an applied voltage of 1000 V [28].

3. Limitations of Current Designs

LT Hick's and MAJ Shrank's thesis work focused primarily on electrode fabrication and growth of CNTs. They therefore devoted less time to the development of a more practical test chamber that combines a user-friendly operation with the required capabilities. As a result, both GEN1 and GEN3 lacked some of the analytical tools needed to provide comprehensive metrics for the CNT FI electrodes.

The issue with the GEN1 test chamber is that there is no parts list included in the thesis writeup from which to reconstruct the apparatus. Coupled with the fact the apparatus is no longer available, it is unknown as to how the sample and grids were mounted in the ionization chamber. This is because, along with the parts list, there are no diagrams illustrating how they were mounted. Also, there was no attempt to measure the mass flow rate of the sample.

The main drawbacks of the GEN2 design are the uncertainty with respect to the gap distance of the electrodes, a complicated sample installation procedure, and the inability to accurately determine the mass flow of the gas through the CNT FI electrode. At first, MAJ Shrank used Kapton washers to set the gap distance. The thickness of the Kapton washers was confirmed using SEM images. However, due to the issues encountered in mounting the sample, he changed from using washers to using layers of Kapton tape applied directly to the substrate. The thickness of a single strip of Kapton tape was measured using a SEM and used for gap distances calculations. However, this technique is based on the assumption that the thickness of all Kapton layers is equal, and that

⁸ The pre-etched hole was a $200\text{ }\mu\text{m} \times 200\text{ }\mu\text{m}$ square hole.

the change in thickness under compression is negligible. Once the sample was mounted, and the ceramic screws tightened, the gap distance could not be confirmed. Considering the fact that gap distances are on the order of a few micrometers, the change in gap distance under compression of a polymeric material could have been significant.

Furthermore, since the mount for the sample was attached to the apparatus, an assistant was needed to mount and demount the CNT samples (Figure 19). This was necessary to prevent damage to the samples, as well as prevent the shearing of the ceramic screws that held the sample in place.⁹ Because of the extra effort and finesse required when mounting/demounting samples, the GEN2 apparatus proved not to be a user-friendly design.

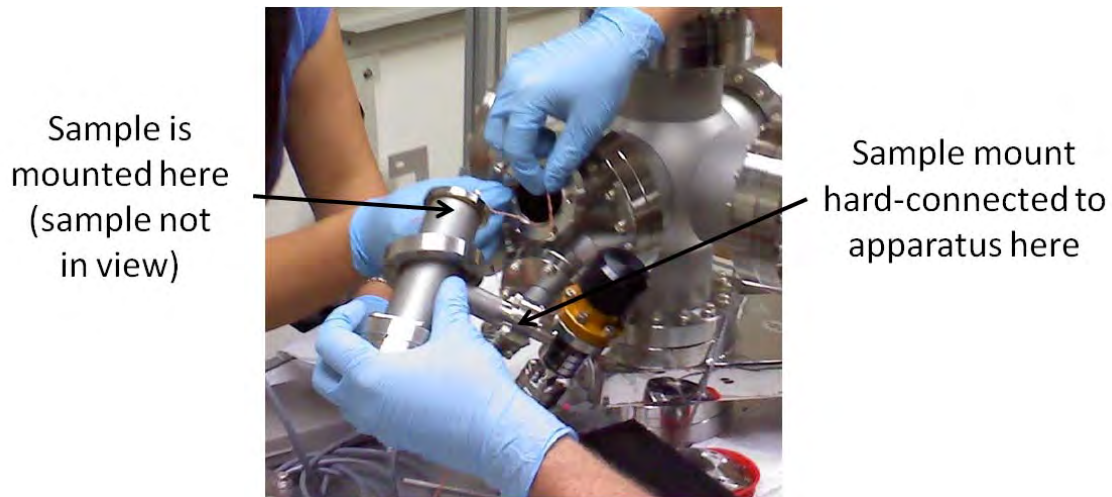


Figure 19 Affixing the test base to the GEN2 chamber (After [28])

⁹ Bryan noted when mounting samples: "It is very easy to brush up on, and therefore ruin, a sample. Additionally, an extra set of hands was very useful when mounting the test base back onto the chamber because it was easy for the mount to slip while mounting the screws, causing the heads of the ceramic screws to shear off [28]."

The mass flow rate was determined using pressure gradients and based upon the assumption that the gas flow operated under the theory of continuum flow. However, the experiments were conducted under vacuum, conditions at which continuum flow theory is not applicable, and free molecular flow equations apply.

a. Comparison of Continuum and Free Molecular Flow

Mass flow rate (\dot{m}) is the amount of mass passing through a given surface per unit time.¹⁰ It is calculated from the density of the gas (ρ), the cross sectional area through which the gas is flowing (A), and its velocity relative to the area of interest (V). If ρ is constant, the practice is an average value is determined for V , yielding the following equation for \dot{m} [32]:

$$\dot{m} = \rho A V_{avg}.$$

Equation 10: General Mass Flow Rate Equation (From [32])

Since ρ and A are the known quantities, the goal is to determine V_{avg} . A few ways V_{avg} is measured are via the use of a pitot-static system, a hot-wire system, or a capillary flowmeter system [32].

These methods share one thing in common: they are based on continuum flow, which is based on the principles of the ideal gas law. The term “continuum” refers to the postulate that the air that surrounds us feels like a continuous medium. However, as the density of a gas decreases, the medium goes from continuous to sparse (i.e., you begin to feel the individual impacts of each molecule). This regime is known as free molecular flow (i.e., low-density flow). The Knudsen number (Kn) is a ‘similarity parameter’ that governs these different regimes. It is defined as the ratio of the mean free path, λ ,¹¹ and a

¹⁰ The mass discussed here is a gas.

¹¹ The mean free path is the average distance a molecule of gas moves between successive collisions.

characteristic dimension of the body in question, L . $Kn > 1.0$ implies free molecular flow, $Kn < 0.03$ implies Continuum Flow, and a transitional regime exists between $0.03 < Kn < 1.0$ [33].

The mean free path is inversely proportional to pressure. Since we are interested in measurements at very low pressures, Kn s are > 1.0 , meaning these measurements involve nearly free molecular flow. Thus, the methods previously discussed do not yield an accurate calculation for \dot{m} . This is because these methods assume a velocity profile of the gas flow similar to that shown in Figure 20 [32]. The flow at the boundaries, referred to as the boundary layer, is zero due to friction. This is not true in the case of free molecular flow. A condition known as velocity slip begins to develop with $Kn > 0.03$ [33]. Velocity slip results in nonzero velocities at the boundaries, which in turn results in an increase in mass flow rate with a corresponding increase in pressure differential. While there are corrections that can be applied to Equation 10, the new test chamber design will utilize a mass flow controller which can properly measure and control mass flow rate at low pressures, thus simplifying mass flow rate determination.

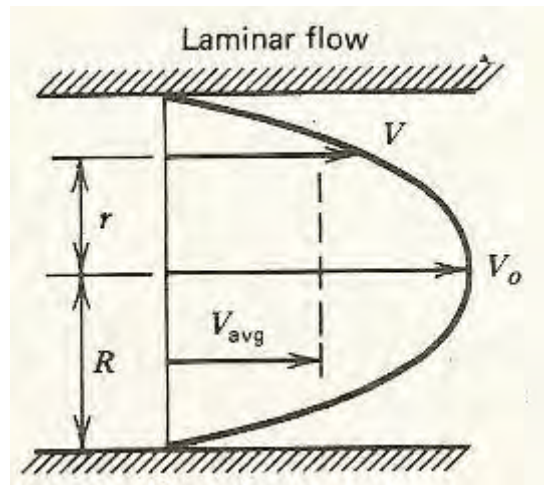


Figure 20 Velocity profile (From [32])

II. OBJECTIVES

The objective of this thesis is to design a user-friendly FI test chamber that provides the analytical capabilities needed to determine comprehensive performance metrics for the CNT FI electrodes. The test chamber must be able to conduct both FE and FI tests, and will incorporate several improvements over the previous test chamber designs developed by NPS students at NASA Ames.

A critical requirement is to enhance the user-friendliness of the test chamber. This will require the apparatus to be operated and manipulated by a single person (no assistance required). It will also require the turnaround time between experiments to be reduced. Components and control software used to operate the apparatus should be largely of a plug-and-play type, with easy-to-use user interfaces.

Another crucial design component is the use of high accuracy volt/current meters, a gap distance controller, and mass flow analyzer. For gap distance, a system that utilizes digital position feedback is required. The position feedback resolution should be at least 1 μm , with a matching repeatability. Also, the operator needs to be able to adjust the gap distance with the apparatus fully assembled. For mass flow rate, a system that calculates mass flow rate independent of pressure is required. This will allow for accurate mass flow rate calculations under vacuum conditions. For the ion current, a high-voltage source-measure unit (HVSMU) is required. This unit supplies the necessary voltage for ionization, and measures the generated ion current, at the same time.

THIS PAGE INTENTIONALLY LEFT BLANK

III. RESULTS AND DISCUSSION

A. DESIGN OF THE NEW TEST CHAMBER

1. Improvements to GEN1 and GEN2

The key inefficiencies to fix are the measurement of the mass flow rate and the gap distance. A thermal mass flow controller (MFC) can be used to accurately measure and regulate the flow of gas through the system. A MFC uses the heat transfer properties of the gas, vice differential pressure, to calculate mass flow rate. This means the measurement is independent of pressure. The gap distance can be determined and adjusted using a system external to the chamber, much like the micrometer used by LT Hicks in the GEN1 apparatus.

The next issue that must be corrected in the new chamber design is user friendliness of the apparatus. It must be ensured that a single user can operate (i.e., changing samples) and maintain (e.g., changing gaskets, chamber repairs) the system, and that the time required to establish the vacuum and to replace sheared ceramic screws that secure the sample (a recurring problem) is minimized. To accomplish this, the sample mount must be designed such that it can be removed entirely from the apparatus. With the sample mount removed, samples can be attached without being constrained by the apparatus. The sample mount could also be designed so as to allow the growth of CNTs directly onto it. The mount for the sample must also be removable. This ensures that in the case when screws are sheared, the mount can be removed and replaced within minutes without having to disassemble the entire apparatus.

Lastly, the turnaround time between experiments needs to be improved. MAJ Shrank's GEN2 apparatus required ~ two hours to reach $1\text{E-}7$ torr, and ~ eight hours to reach $1\text{E-}8$ torr. Designing the apparatus so that the total chamber volume is minimized, as well as having vacuum pumps connect at the front and

back end of the apparatus, will reduce the vacuum draw-down time, thus reducing the overall time needed to conduct ionization experiments with different samples.

2. Generation 3 Test Chamber

With the limitation of GEN1 and GEN2 in mind, I enlisted the help of Mr. Jay Adeff (Research Assistant, Mechanical and Aerospace Engineering Department, NPS) to assist in creating the first option for the next generation, Generation 3 (GEN3), of the test chamber for use at NPS. Mr. Adeff's recommendation was to design a "twist-to-adjust" chamber. The idea behind this design is to make the downstream end of the chamber threaded, so the gap distance can be adjusted by simply twisting the downstream section of the chamber (Figure 21). The upstream section of the chamber resembles a grooved-ASA half-nipple. The next part is a removable mount upon which the sample is mounted. The sample is attached to the mount via an electrically conductive adhesive (i.e., silver or carbon-based epoxy). This mount is sandwiched between the upstream and downstream sections of the chamber. The threaded portion of the downstream section is made of non-conductive material, so the gap adjuster is electrically isolated from the sample; it is pressed into the flange. The gap adjuster holds the accelerator grid, and threads into the downstream flange. For power, a positive potential is applied to the sample mount, while a negative potential is applied to the gap adjuster.

This design satisfies the requirements of a removable sample mount for easier sample exchange and reduced overall volume. However, there are issues with this design. First, since the gap adjuster translates and rotates, the attachment at the downstream end has to accommodate that motion. Also, the gap adjuster has to be electrically isolated at both ends. This is because the negative potential must be applied to the external surface of the gap adjuster (putting a charge on the entire section), so as to provide the accelerator grid with a negative potential. This isolation requirement is already satisfied on the

upstream end by the non-conductive thread insert. To isolate the downstream end, a threaded mount, made of non-conductive material, has to be designed that can connect to the rest of the apparatus. A possible solution for this is show in Figure 22.

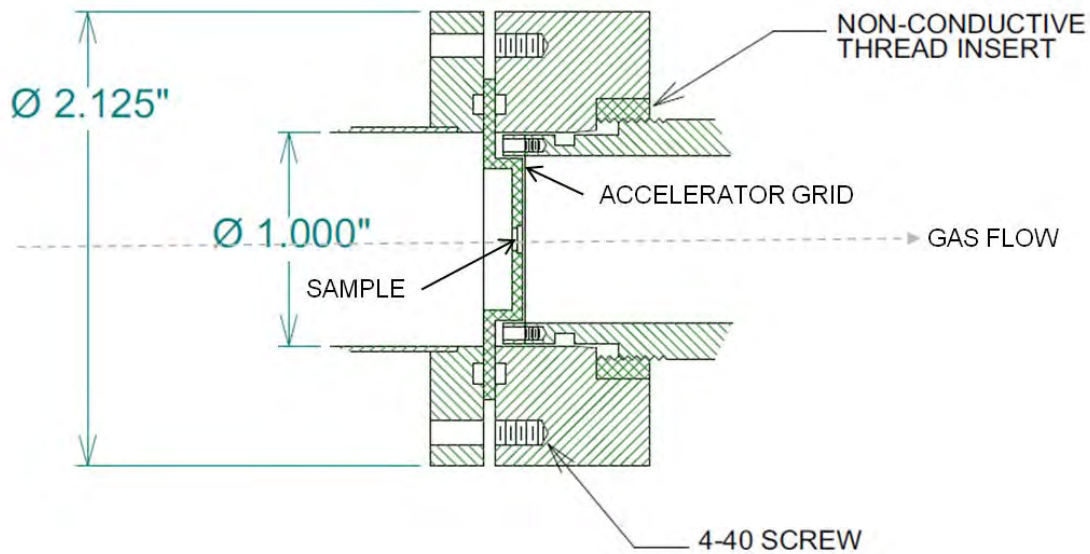


Figure 21 GEN3 ionization chamber

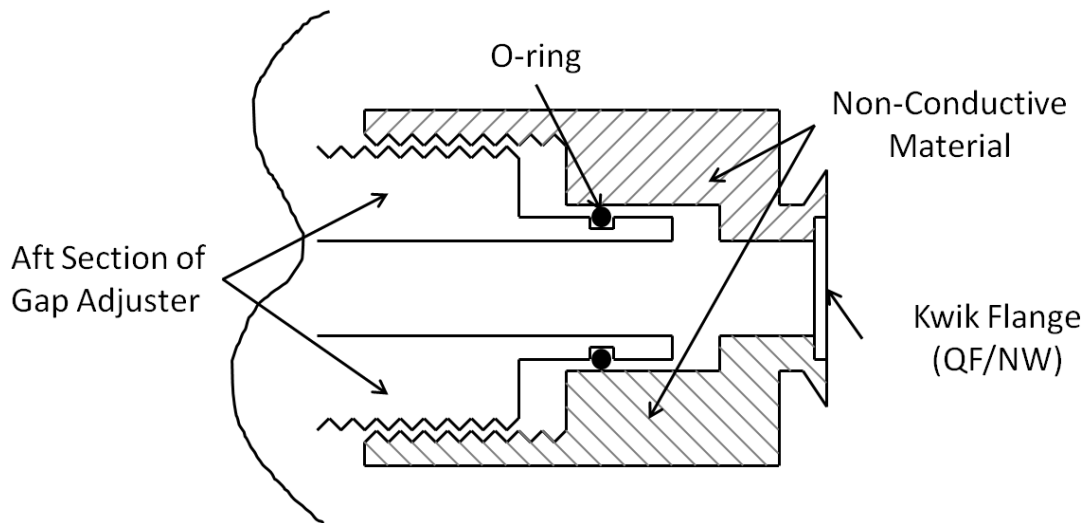


Figure 22 Downstream connection of gap adjuster for GEN3 apparatus

Second, the sample mount needs to be electrically isolated. The sample mount itself must be conductive to allow the electric potential applied to it to reach the sample. However, since the upstream and downstream flanges are metal as well, they also will have the potential applied to them. This is not desirable, because it could create an unsafe work environment if high voltages are applied. It could also damage equipment that has a conductive connection to the rest of the apparatus. A solution to this could be to make the upstream and downstream flanges entirely out of non-conductive material. However, this material may not be as durable as metal flanges. Another solution could be to break the sample mount into two pieces (Figure 23).

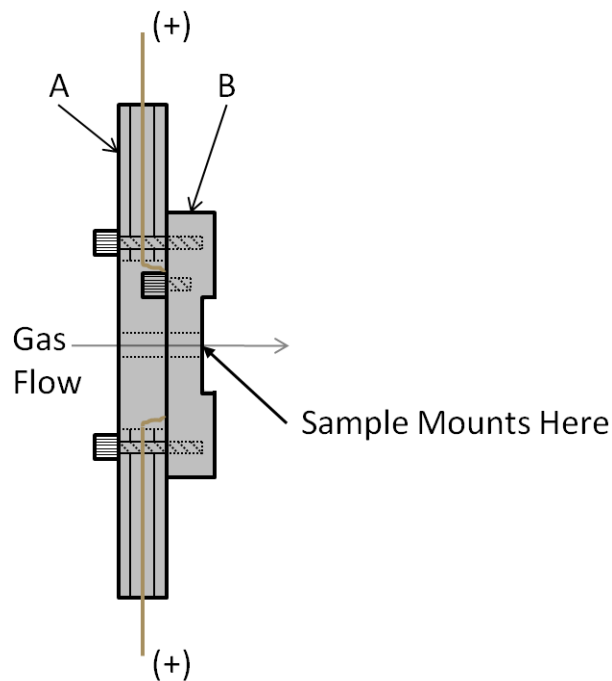


Figure 23 GEN3 sample mount option

With this option, the upstream and downstream flanges sandwich flange A. The sample itself mounts to flange B. B is electrically isolated from A by Kapton. A has channels drilled into it to allow wires to be passed through and connected to the back of B. The channels are vacuum-sealed with a vacuum grade epoxy. This design yields an added advantage. Since the samples are

attached to the mount via adhesive, they will be damaged if attempts are made to remove them (chemically, or physically). With this design, samples remain permanently attached to the mount, and each sample has its own mount. Thus, after a sample is attached to the mount, it does not have to be touched again. This reduces the possibility of damaging the sample through handling. In addition, the mounts can be designed so they can fit in growth chambers.

Another issue concerns the linear translation required for experiments. Based on MAJ Shrank's previous work, the range of motion is expected to be no greater than 100 μm . With that, a translational resolution of 1 μm is desired. While a micrometer screw is capable of achieving this resolution, its use would prevent the gas flow from being linear throughout the apparatus. An option is to use a dial indicator with a plate attached to the gap adjuster (Figure 24). As the gap adjuster rotates, the plate pushes against the dial indicator, indicating displacement from some zero-position.

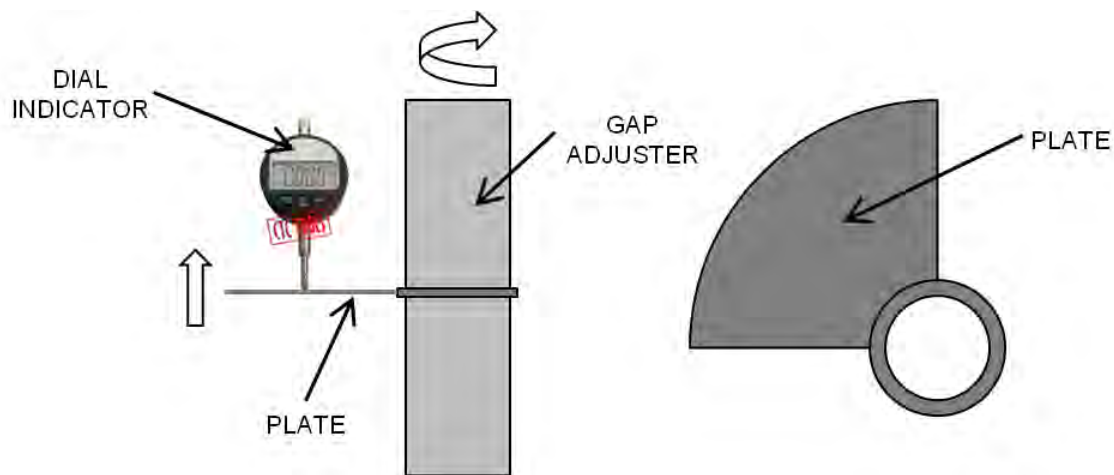


Figure 24 GEN3 gap distance determination

Making gap adjustments on the order of micrometers by simply twisting the gap adjuster is impractical, though. The first issue is the thread pitch. Since the desired range of motion is 100 μm , the necessary thread pitch required is 254

threads per inch (TPI).¹² The concern with this magnitude of pitch is the fact that the thread depth is so small; it will be easy to cross-thread the gap adjuster when changing samples, thus damaging the threads (this assumes 254 TPI can even be made). Second, since the plate used for measuring gap distance is intended to rotate 360° per 100 µm of linear translation, the apparatus setup will have to accommodate this. This means, depending on the radial size of the plate, a section may have to be removed from the apparatus table to allow for plate clearance. One option is to reduce the thread lead to 90° per 100 µm. This would reduce the thread pitch to ~64 TPI, and reduce the plate to ¼ of its angular size (Figure 24). This eliminates the need for cutting the table. However, now 1 µm of translation equates to ~ 1° of rotation, still an impractical situation to do by hand with the gap adjuster at such a small diameter. A solution could be to increase the radial length of the plate, and make gap adjustments by moving the plate, directly. This would increase the arc distance required to be traversed to achieve a desired linear translation, thus increasing the fidelity of rotation. Overall, this solution is limited to 100 µm of linear motion. If a greater distance is needed, a section of the table will still have to be removed for plate clearance. The inability to determine an effective and efficient solution to adjust the gap distance resulted in abandoning this design.

The final design for the ionization chamber solved the issue of being able to make gap adjustments with the apparatus fully assembled, as well as instantaneously determining the gap distance. It utilizes the 2-part sample mount discussed earlier (Figure 23), making the system more user-friendly. It also incorporates a MFC for instantaneous mass flow measurements.

a. *Linear Shift Mechanism with Linear Potentiometer (LSM38–50-SS-LP-UP, Kurt J. Lesker Company)*

The primary component of the GEN3 ionization chamber design is a linear shift mechanism (LSM) with a linear potentiometer (LP) attached (Figure

¹² This assumes 100 µm of linear translation for 360° rotation of the gap adjuster.

25). The LSM supports a removable bellows, which serves as the actual ionization chamber. A stepper motor is used to adjust the distance between the two flanges of the bellows; one flange remains stationary while the other translates linearly, thus allowing for accurate gap adjustments between the electrodes. The LP, which has a resolution and repeatability of 2 μm , provides instantaneous position feedback of the translating flange with respect to the stationary flange. The size of the bellows is $\sim \frac{1}{2}$ in larger in diameter (1.57 in inner diameter) than the GEN3 design. This size was chosen to ensure easy handling and accessibility, while keeping the chamber volume reasonably small. Too small of an inner diameter would have resulted in a very small sample mount, resulting in the setup being too petite to handle.

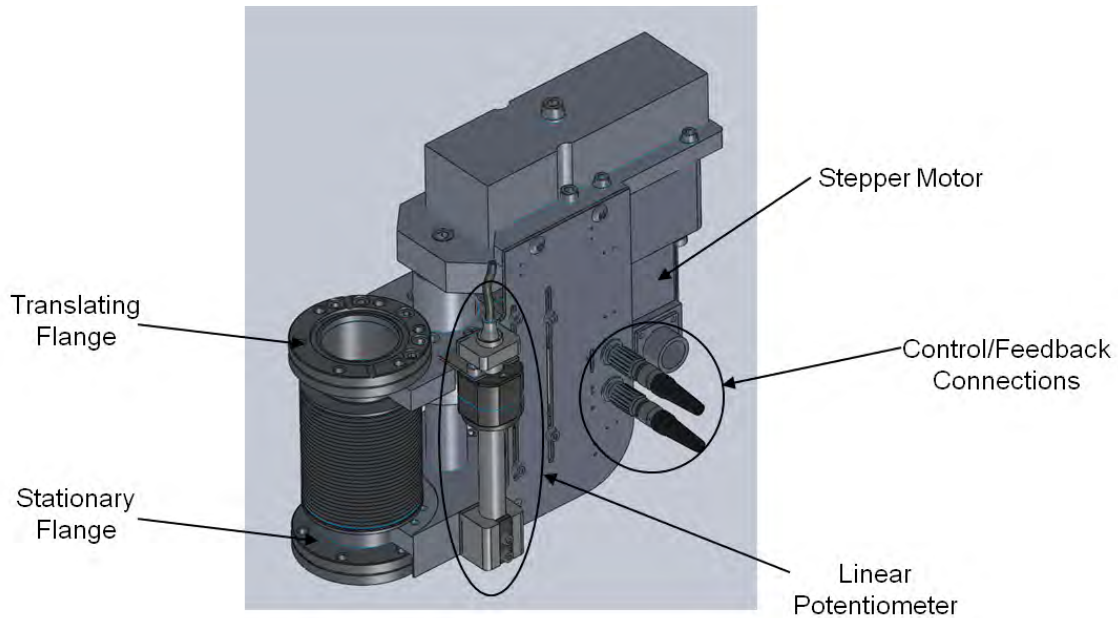


Figure 25 Linear shift mechanism with linear potentiometer

The 2 μm resolution is greater than the desired resolution of 1 μm . However, given the capabilities of the system, the tradeoff is acceptable, accurate experiments can still be conducted with this added error.

b. Electrode Mount

The Electrode Mount (Figure 26) will mount the electrodes (in this case, the accelerator grid and CNT sample electrodes), via the use of an electrically conductive adhesive. Electric potential will be applied directly to the mount. It will be electrically isolated from the rest of the apparatus via the use of Kapton washers.

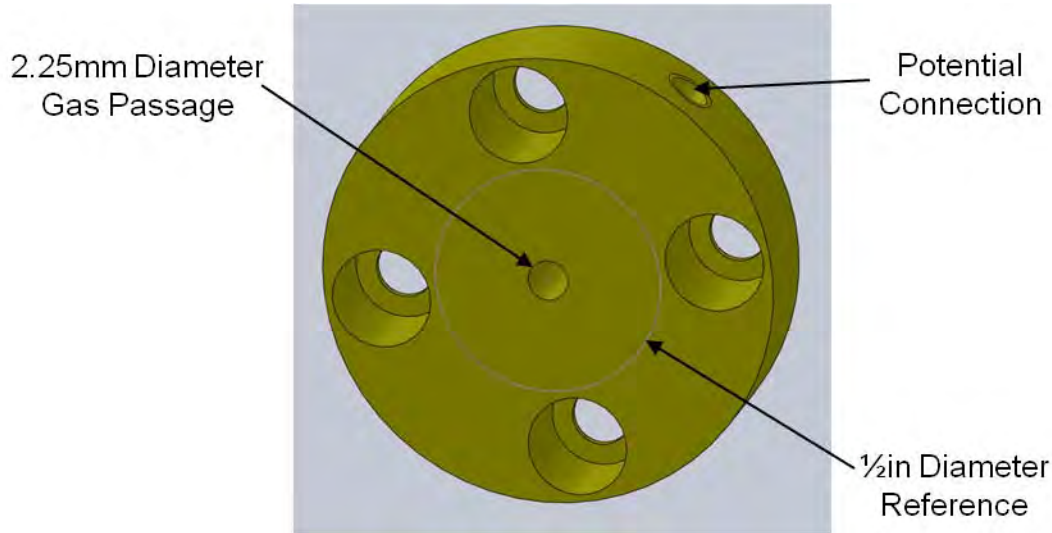


Figure 26 Electrode mount

The gas passage size can be adjusted to allow for samples of varying sizes. The sample/electrode must fit within a $\frac{1}{2}$ in diameter to use this mount (Figure 26). If a larger size is required, the entire apparatus will have to be resized to accommodate. Currently, the Electrode Mount is sized to accept 3.05 mm diameter TEM grids, with CNT arrays grown directly on them.¹³

c. Sacrificial Mount

Sacrificial Mounts (Figure 27) are mounted in between the Electrode Mounts and their respective mounts. They are included because of the possibility of sheared screws. The screws that must be used to attach the electrode mounts must be non-conductive (i.e., ceramic, or plastic). As

¹³ The "flange" on these grids has a thickness of 400 nm.

demonstrated in MAJ Shrank's thesis, these screws are easily sheared. With the sacrificial mount, if a screw is sheared, the sacrificial mount can be removed without disassembling the entire apparatus. A replacement mount can be used in its place to continue experiments, while the fouled mount has the screw removed. This limits the time loss due to sheared screws to a minimum, making the test system more efficient and user-friendly.

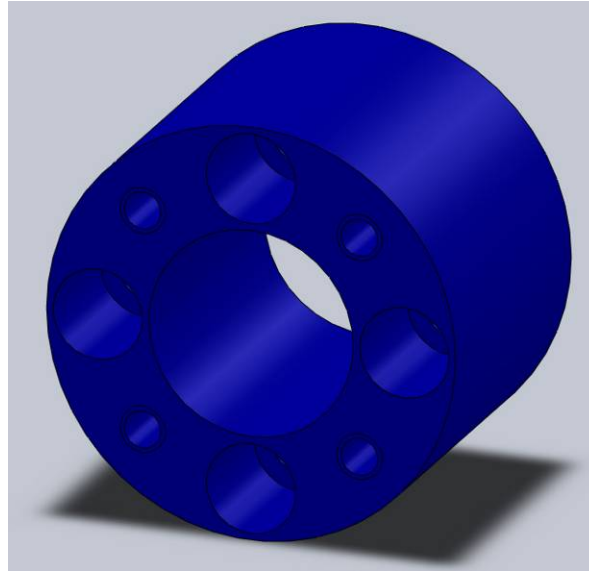


Figure 27 Sacrificial mount

d. Accelerator Grid Electrode Mount – “Top Hat”

The top hat is the unit upon which the accelerator grid electrode will be mounted (Figure 28). This mount will connect to the stationary end of the LSM, remaining fixed during gap adjustments. It is made from a double-face conflat flange. A 1 in outer diameter cylinder, with a $\frac{1}{2}$ in inner diameter channel, is attached to it. The passage drilled from the outside flange to the base of the Top Hat is where the wire providing negative potential to the electrode mount will be routed. Figure 29 shows how the Top Hat will mount with the sacrificial and electrode mounts.

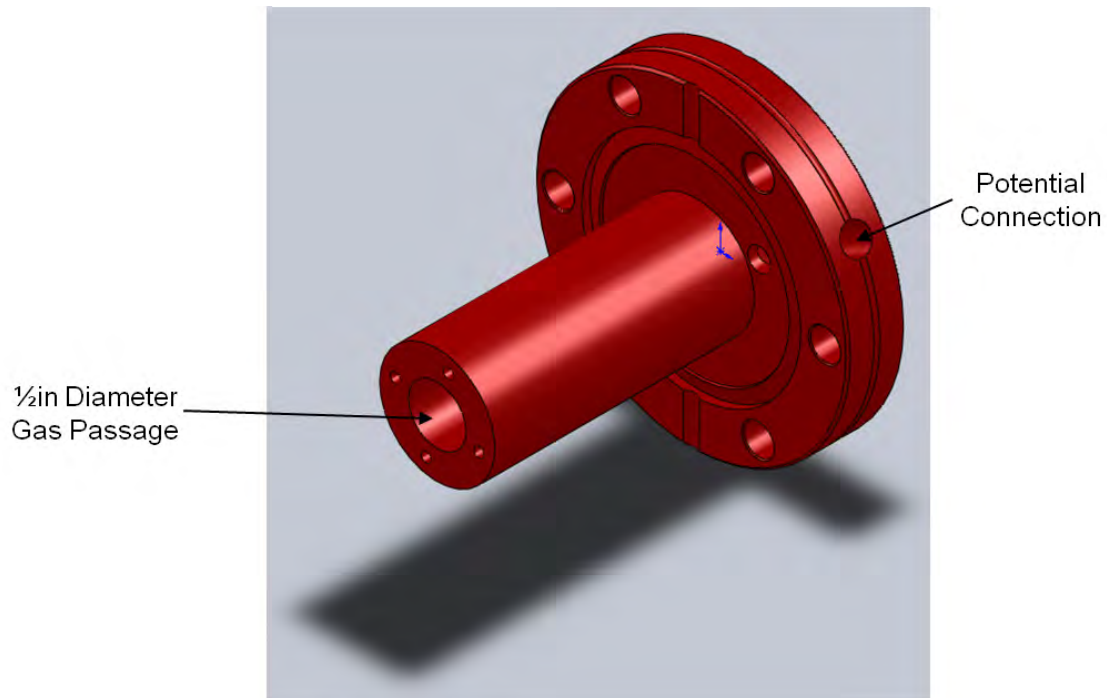


Figure 28 Top hat

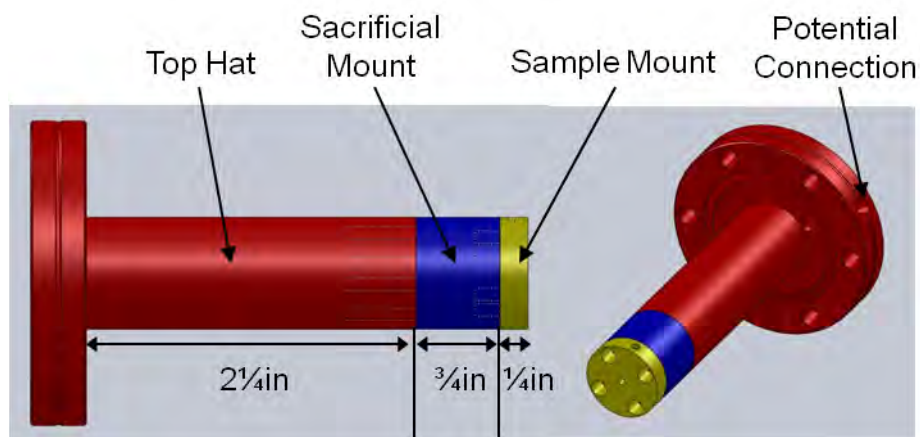


Figure 29 Top hat with sacrificial mount and electrode mount attached

e. Sample Electrode Mount

This mount holds the samples to be tested (Figure 30). It attaches to the translating end of the LSM. It is made from a double-face conflat flange, with a 1/2 in diameter gas passage drilled into it. It has a wire passage for the wire that will provide the positive potential to the electrode mount. A sacrificial mount

will be mounted between the sample electrode mount and the electrode mount.
Figure 31 shows how these components will be mounted.

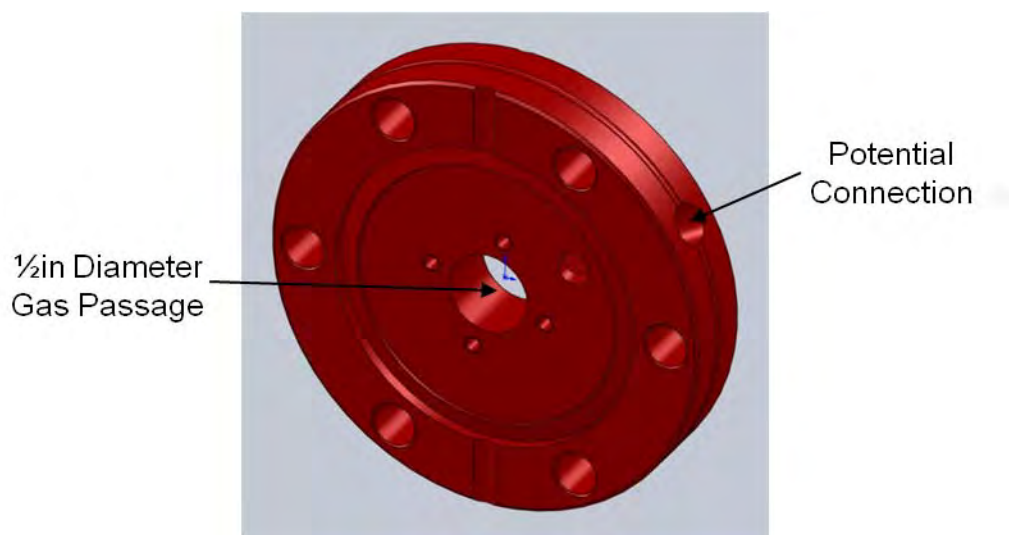


Figure 30 Sample electrode mount

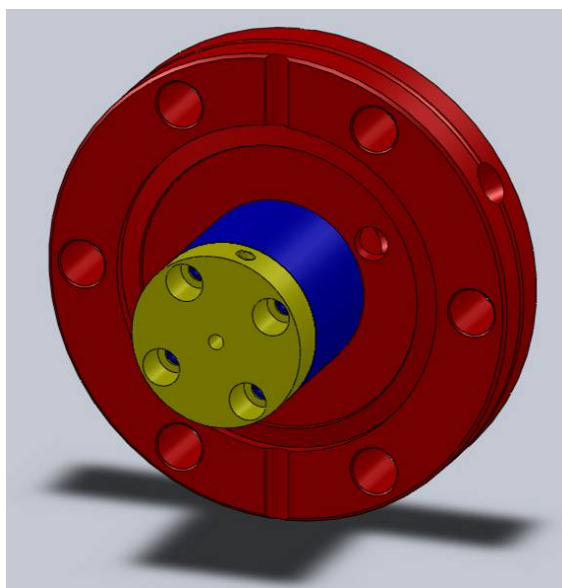


Figure 31 Sample mount with sacrificial mount and electrode mount attached

f. Thermal Mass Flow Controller (C100, Sierra Instruments)

Accurate measurement and control of the mass flow is provided by a thermal MFC (Figure 32). A thermal MFC determines mass flow rate based on the heat transfer properties of the gas being used. A portion of the gas flow entering the MFC is directed through a capillary tube. This tube has two resistance temperature detector (RTD) coils wrapped around it. The gas takes heat from the upstream coil and passes it to the downstream coil. The MFC takes this difference in temperature, along with the coefficient of specific heat for the gas in use, and calculates a mass flow (Figure 33). The MFC is operated using a pilot module. A detailed description of the procedures required to operate the MFC are located in Appendix B.



Figure 32 Thermal mass flow controller (left) with pilot module (right)

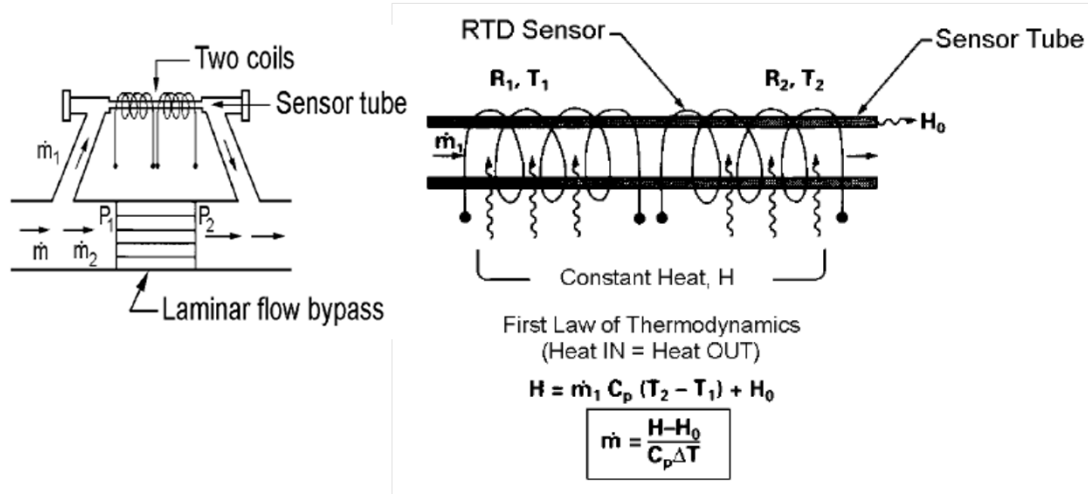


Figure 33 MFC mass flow rate determination (From [34])

g. High-Voltage Source-Measure Unit (Keithley 237)

The HVSMU will provide the voltage that will be applied to the electrodes (Figure 34). It is capable of sourcing voltage and measuring the generated current, in one unit. The maximum voltage producible is 1100 V, which produces a maximum current of 10 mA. The unit can be controlled locally via its front panel, or remotely via a computer using the program LabView. In the remote configuration, LabView can extract the generated voltages, and associated currents, from the HVSMU for data analysis. The unit can generate either a constant DC source, or a “sweep” source, where the voltage is varied over time. Procedures for operating the HVSMU are located in Appendix C.



Figure 34 Keithley 237 high-voltage source-measure unit

h. Complete Test Stand

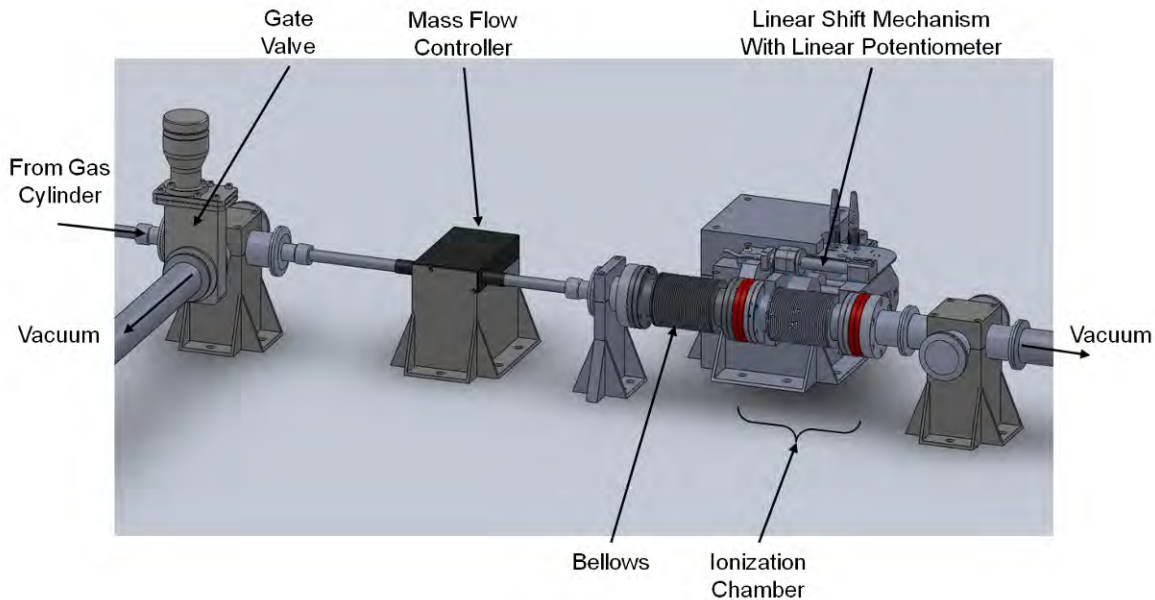


Figure 35 Complete GEN3 test stand (HVSMU not pictured)

The completely assembled test stand is shown in Figure 35. The propellant gas enters the apparatus at a 4-way cross (from the left), passes through the MFC, where mass flow rate is metered and controlled, into the ionization chamber. A gate valve is attached to the 4-way cross at the front end of the apparatus. This gate valve is an on/off valve that controls vacuum flow at the front end of the apparatus. This vacuum access point is used to decrease the vacuum draw-down time. The system will reach operating pressure faster by drawing vacuum at both ends of the apparatus, thus reducing turnaround time between experiments. The apparatus supports were designed in SolidWorks and created using NPS's 3D printer. They are made of a polycarbonate plastic. Figure 36 shows how the sample electrode mount and accelerator grid electrode mount are mounted within the ionization chamber.

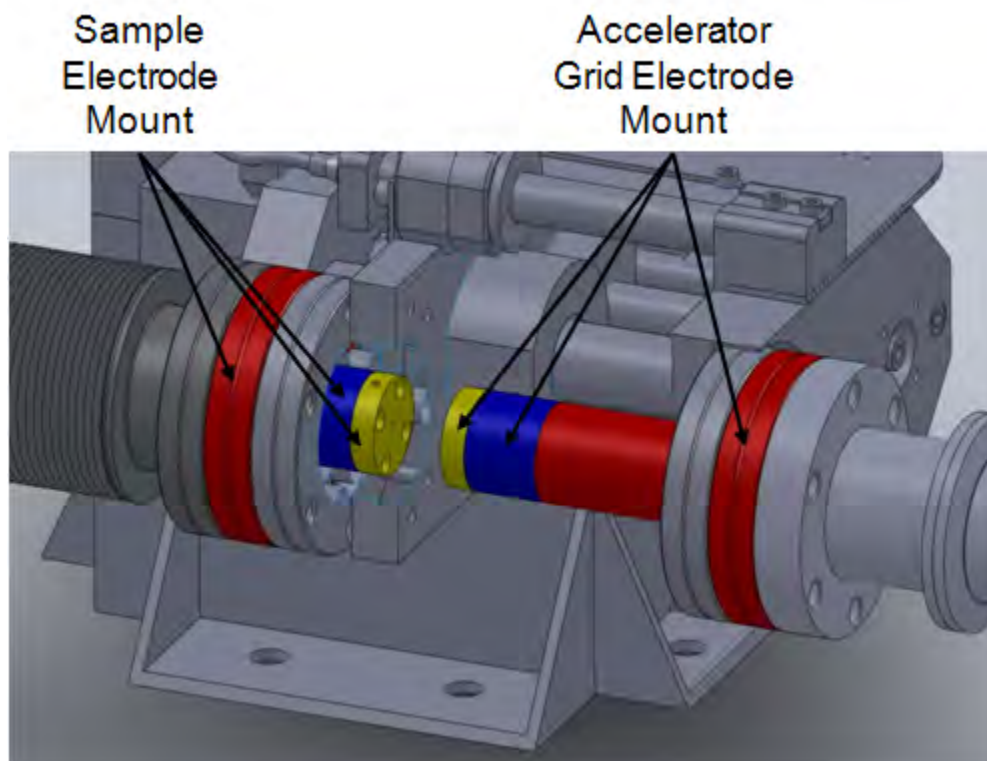


Figure 36 Sample electrode mount and accelerator grid electrode mount within ionization chamber (LSM bellows suppressed to allow for viewing of mounts)

This design satisfies all requirements mandated in the previous sections. First, the design is user-friendly. Once samples are mounted to electrodes, they no longer require direct contact. This greatly reduces the possibility of damaging samples, especially during installation. These samples are then mounted to the sample electrode mount, which can easily be removed from the apparatus. This makes installation easier, and further reduces the possibility of sample damage. Sacrificial mounts are used in between electrode and sample/top hat mounts. These prevent time lost due to sheared plastic/ceramic screws used to secure the electrode mounts. Without this mount, if a screw is sheared in the top hat, the entire apparatus will have to be disassembled to remove the fouled top hat. The sample electrode mount and upstream bellows connect via studs secured to the translating flange of the LSM. This further makes installation easier, because the sample electrode mount and

bellows flanges simply slide and align into place over the studs. The user does not have to keep three flanges aligned while attempting to secure them. Thus, it requires only one user to exchange samples (Figure 37).

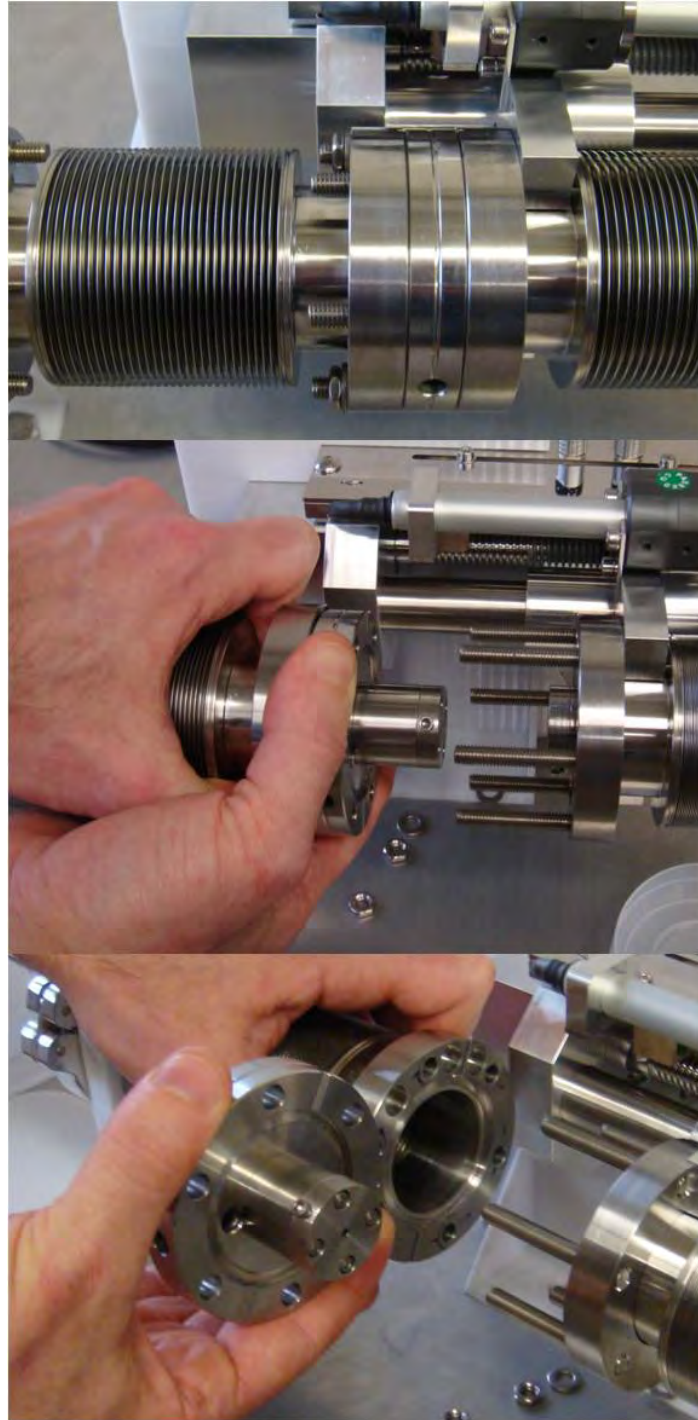


Figure 37 Sample exchange

Second, high accuracy, plug-and-play components were chosen to measure the required parameters (mass flow rate, applied voltage, ion current, electrode gap distance). The Sierra Instruments MFC yields real time measurement and control of the propellant flow, while its external control unit has a user-friendly interface. The Keithley HVSMU controls the applied voltage and measures the generated ion current. It has a user-friendly interface, via both its front panel and through LabView. Data can be pulled directly from the HVSMU via LabView for data analysis. The Kurt J. Lesker LSM with LP externally controls the electrode gap distance, as well as gives live measurement of that distance.

Third, the turnaround time was decreased. This was accomplished by reducing the internal volume of the chamber by 70%. The GEN3 chamber has an internal volume of $\sim 110 \text{ in}^3$, while the GEN2 chamber has an internal volume of $\sim 375 \text{ in}^3$. The system also has vacuum connections at the upstream and downstream ends of the apparatus. This reduces the time required to bring the apparatus down to the required operating pressure.

An added feature of this design is the fact it is highly modular. Minus the Sacrificial, Electrode, and 3D printer mounts, the apparatus is composed of commercial, off-the-shelf parts. This keeps the system cost low, and makes future adjustments to the design easier, using standard parts. Addition components, such as pressure transducers, can also be added to the 4-way crosses, along with a gas supply at the downstream 4-way cross to simulate varying altitudes. Lastly, a Mass Flow Meter (MFM) can be included in between the downstream 4-way cross and the ionization chamber to ensure the mass flow rate going into the chamber matches the mass flow rate leaving it.

B. FIELD EMISSION AND FIELD IONIZATION TESTING

FE and FI tests will be conducted using a CNT sample grown on a TEM grid to confirm the GEN3 design functions properly. This sample was created by CAPT Allan Wold, USMC, during his thesis at NPS [35]. Tests will be conducted at a vacuum pressure of 1E-7 torr. This is a sufficient vacuum to simulate conditions in outer space.

1. Field Emission Testing

The goal of the FE tests will be to determine the field enhancement factor, β , of the CNT in accordance with Fowler-Nordheim theory. These tests will be conducted at vacuum pressure, with no propellant¹⁴ flowing. A negative potential will be applied to the sample electrode; a positive potential will be applied to the accelerator grid electrode. Both potentials will be applied to the wires that attach to the Electrode Mounts via the leads external to the chamber. The gap distance will initially be set to 50 μm , then incrementally decreased by 10 μm to a final distance of 10 μm .¹⁵ For each gap distance, the “sweep” function of the HVSMU will be used to apply 0 to 1100 V. This will yield for each gap distance the ~ voltage the CNTs begin to field emit.¹⁶ The generated currents and applied voltages will then be plotted using Equation 4: Plottable form of Fowler-Nordheim equation (corrected). If the plot is linear, then the CNTs field emit in accordance with Fowler-Nordheim theory. β can then be calculated from the slope of the plot. This should yield a range of β s by which to characterize the field enhancement provided by the CNTs.

¹⁴ The propellant being used for these experiments is pure Argon gas.

¹⁵ LT Hicks used a range from 10–100 μm for his initial tests [18]. His results showed a trend of increasing current for a decrease in gap distance, in accordance with Equation 9. MAJ Shrank did most of his experiments at ~100 μm [31]. Since the goal is strictly to show the apparatus works, the number of data points was halved.

¹⁶ Also referred to as the “turn-on” voltage.

2. Field Ionization Testing

The goal of the FI tests will be to demonstrate the feasibility of field ionization through CNT-covered grid electrodes while providing reliable ionization efficiency data and other critical performance metrics. The results of these experiments will yield the MUF, which will confirm whether or not a CNT-based IT is feasible. FI testing will be conducted at vacuum pressure, with propellant flowing. A positive and negative potential will be applied to the sample and accelerator grid electrode; respectively. Both potentials will be applied to the wires that attach to the electrode mounts via the leads external to the chamber. The gap distance will initially be set to 50 μm , then incrementally decreased by 10 μm to a final distance of 10 μm . For each gap distance, the “sweep” function of the HVSMU will be used to apply 0 to 1100 V. The objective is to determine for each gap distance the applied voltage at which the Argon gas is ionized.¹⁷ The mass flow rate will remain constant at 10 $\frac{\text{gram}}{\text{hr}}$ ¹⁸ during the experiments.¹⁹ If the test reaches saturation, noted by a loss of current with all other parameters present, then the mass flow rate can be adjusted. The measured current can then be compared to the maximum theoretical current to yield a preliminary MUF for the CNT sample.²⁰

17 This is the voltage at which current starts being generated.

18 The resolution of the MFC is limited to 250sccm. This equals 6.9E-6kg/sec for Argon, which cannot be resolved by the Pilot Module, nor the MFC software. Thus, units of grams/hr had to be used. 250sccm equals 24.83 grams/hr for Argon.

19 At this point, it is unknown what mass flow rate will cause the experiments to saturate. It is possible that the internal electric field associated with the ion cloud can oppose the electric field generated by the accelerator grid electrode when too many charges of the same sign try to pass simultaneously through the accelerator grid electrode. This saturation value is known as the space-charge-limited current [1].

20 These preliminary experiments are intended primarily to test the GEN3 apparatus for proper operation, not to optimize the ionization capability of the CNT sample. Thus, this preliminary MUF is not an optimized value, and the feasibility of a CNT-based IT should not be based solely on this MUF value.

THIS PAGE INTENTIONALLY LEFT BLANK

IV. CONCLUSIONS AND OUTLOOK

A. CONCLUSIONS

This thesis succeeded in designing and building a more user-friendly ionization test chamber that provides the analytical capabilities needed to determine critical performance metrics of the CNT FI electrodes. The GEN3 design can be operated in FE and FI mode and is the key to determining the feasibility of CNT-based IT, in general.

First, the GEN3 is more user-friendly compared to previous chamber designs, as it is capable of being operated by a single user. It has an internal volume of that is 70% smaller than the GEN 2. Lastly, the electrode mounts are designed with a sacrificial mount to minimize time loss due to sheared mounting screws.

Second, the components chosen to operate the system are plug-n-play, with easy to use interfaces. Each of these components is used to measure a specific performance metric. With a resolution of 2 μm , the LSM with LP externally controls and measures the gap distance between the electrodes. This component is also capable of adjusting the gap distance while the apparatus is fully assembled. The MFC is capable of measuring the mass flow rate of the propellant, independent of pressure. The HVSMU is capable of applying the necessary voltage for FE and FI, while measuring the generated current for both instances.

Unfortunately, final FE and FI testing of the GEN3 apparatus could not be conducted in the scope of this thesis due to unforeseen problems with the LSM. During final installation and testing, it was discovered that the ultimate resolution of the LP is not the 2 μm stated by the manufacturer, but is actually 12 μm . The 12 μm resolution is not sufficient for FE and FI testing and the item has to be replaced.

The issue was discovered after the apparatus was fully assembled, and initial operational tests of the LSM were being conducted. After two weeks of troubleshooting tracking and communication errors, the manufacturer of the LSM learned from one of its component suppliers that the employed combination of stepper motor controller and LP can only provide a best resolution of 12 μm .

A potential alternative is to use a LSM with a linear encoder (LE) for position feedback (possibly supplied by Thermionics). This LE will have the desired resolution and repeatability of 1 μm .

Once this new unit is purchased, it is estimated to take three months to have the apparatus fully tested for proper operation. The first month will involve redesigning the mount for the LSM, and testing the LSM and LE for expected motion and position feedback. Vacuum leak checks will also be conducted during this month. The second month will involve conducting the FE and FI tests with CNT samples. The third month will involve any necessary troubleshooting that may be required.

B. OUTLOOK

1. Multi-Hole Electrode Mount

Currently, the electrode mount is sized for only one TEM grid. Because there is enough room on the mount for more than one grid, multi-hole grids should be investigated. Multi-hole grids will allow a higher gas flow through the electrode mount, resulting in increased ionization and higher current, and thus, an increase in the MUF. Figure 38 shows a possible seven-hole electrode mount.

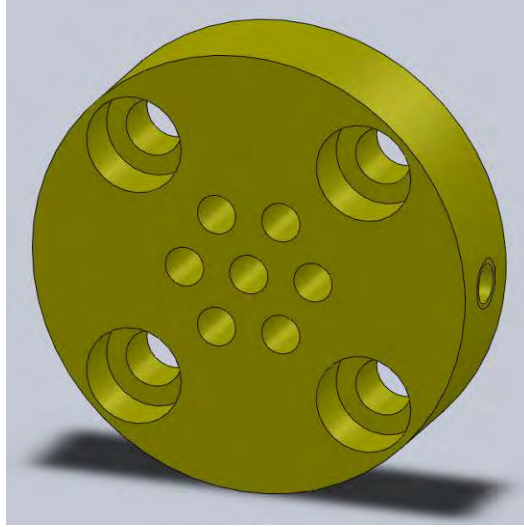


Figure 38 Seven-hole electrode mount

2. Non-Conductive Electrode Mount for Accelerator Grid

For FI testing, the entire electrode mount for the accelerator grid is negatively charged. This means the ionized propellant can be attracted to anywhere on the mount.²¹ This could result in the chamber becoming saturated by propellant that does not go through the accelerator grid electrode. The ions could also build up on the surface of the mount, resulting in a possible electrostatic discharge. A mount made out of a non-conductive material, with a channel for connecting the potential input to the electrode, should be investigated. This will limit the applied potential strictly to the grid electrode.

3. Mass Flow Meter Downstream of Ionization Chamber

To confirm all inputted gas is leaving the apparatus, a MFM can be installed in between the exit of the ionization chamber and the downstream 4-way cross. The assumption with the GEN3 design is that all gas molecules entering the apparatus are leaving the apparatus. As discussed in Section IV.B.2, this might not be the case. Some of the propellant may be attracted to the Accelerator Grid Electrode Mount, or, since the flow direction of the propellant

²¹ Minus the non-conductive mounting screws.

through the ionizing electrode is not guaranteed to be normal to the electrode, propellant may get “trapped” within the ionization chamber. The GEN3 design does not allow for a channel that surrounds the Electrode Mounts, which would contain the flow of propellant. The inclusion of the MFM will yield how much propellant is actually leaving the ionization chamber.

4. Downstream Gas Input for Altitude Variation

The ability to simulate various altitudes via a back-pressure input can yield the affect this has on the performance of the sample, and the flow rate through the apparatus. The downstream 4-way cross has two open connections that can be used for simulating various altitudes. A pressure transducer and a gas input line can be connected to these ports, with a gate/shut off valve before the gas line.

5. Jog Box for Sample Changes

The inclusion of a Jog Box with Joystick can further ease the changing out of samples (Figure 39). A Jog Box allows for moving the LSM via a separate hand-held controller, vice commands inputted via the keyboard. It simply moves the translating flange fore and aft. Flange position is still referenced via the computer interface.

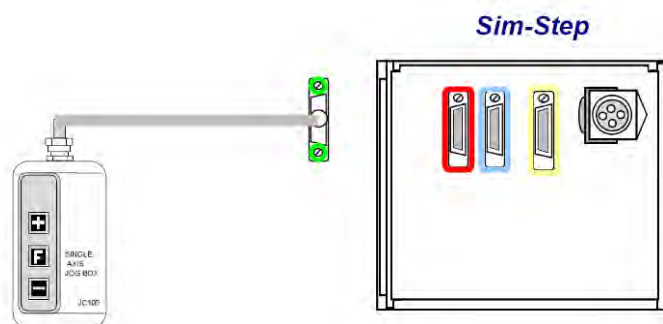


Figure 39 McLennan JC100 Jog Box

6. Replace Upstream Bellows with 100mm Travel Bellows

Replacing the upstream 50 mm travel bellows with a 100 mm travel bellows will make the exchange of samples easier. The 50 mm bellows was used because it is the same bellows connected to the LSM. Thus, both bellows have the same amount of travel. However, the clearance needed to remove the sample mount, with the sacrificial mount attached, requires the upstream bellows to be almost fully compressed. This requires a significant effort. This problem will be solved by replacing the 50 mm bellows with a 100 mm bellows. The 100 mm travel bellows has more travel with which to compress the bellows during sample mount removable and installation, thus reducing the effort required to compress the bellows, as well as increasing the clearance available to remove the sample mount.

7. Linear Encoder for Position Feedback

The resolution of the supplied LP is much higher than what can be used for FE and FI experiments. A LE can achieve the desired 1 μm resolution and repeatability, but must be operated differently from the LP. A LE must first reference itself to some “zero reference” position. Distance is then measured from that zero reference to determine the current position. Also, if the LE loses power, it “forgets” where it is, and must re-reference the zero position before returning to the desired position. The LE can be used in the same manner as the LP. Gap distance would be determined using the same procedures as the LP.

THIS PAGE INTENTIONALLY LEFT BLANK

APPENDIX A. MECHANICAL DRAWINGS

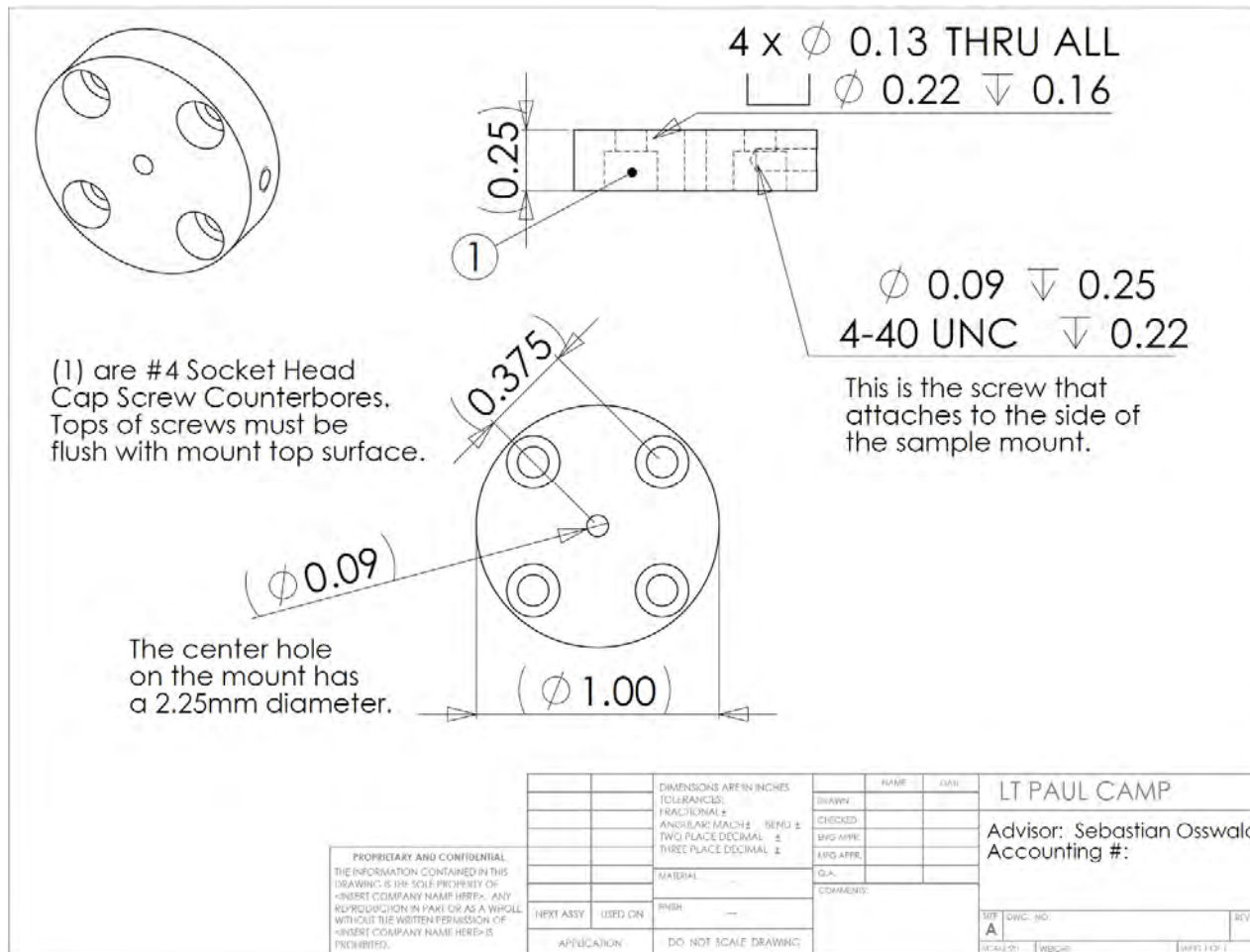


Figure 40 Electrode mount

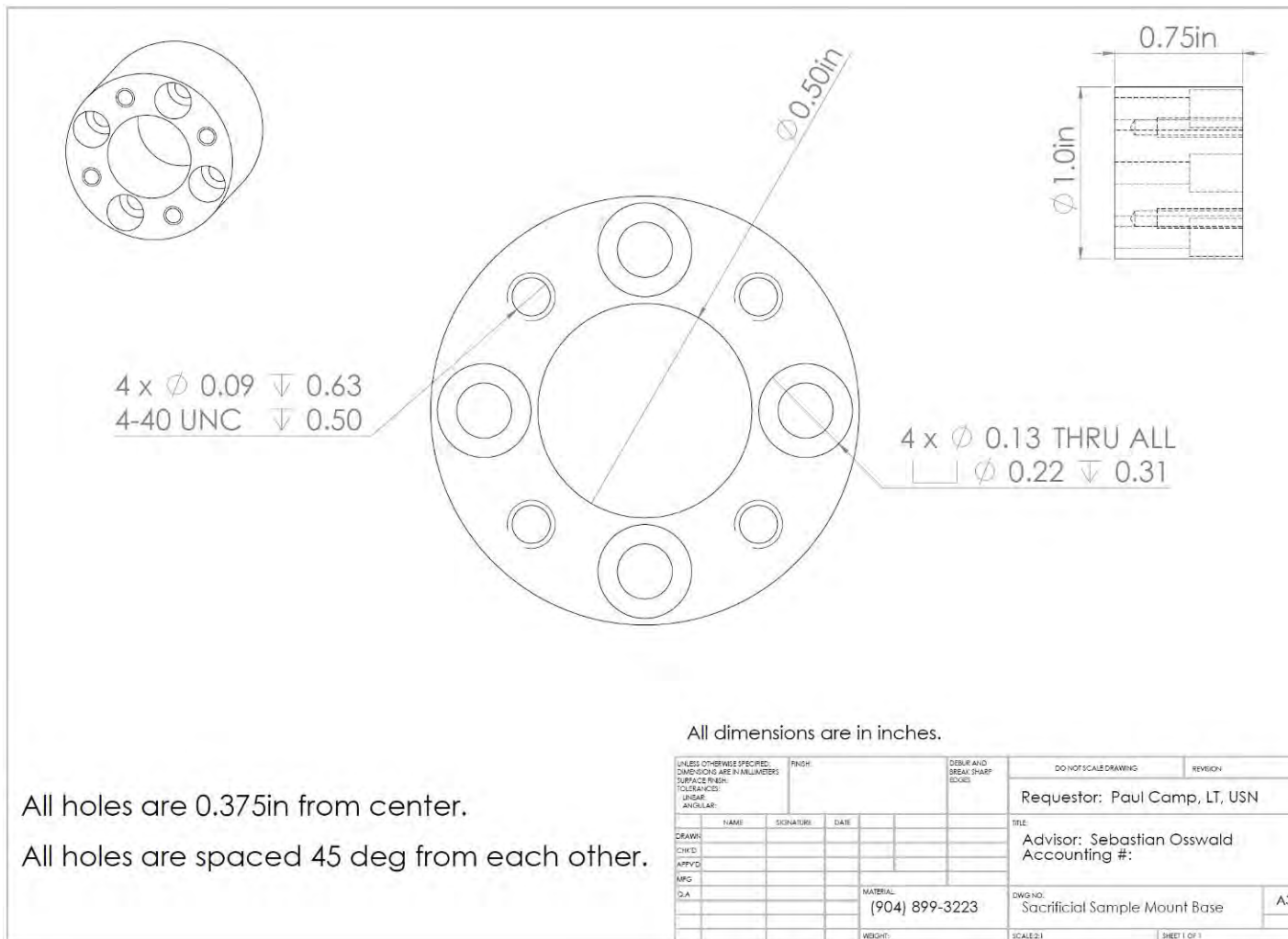


Figure 41 Sacrificial mount

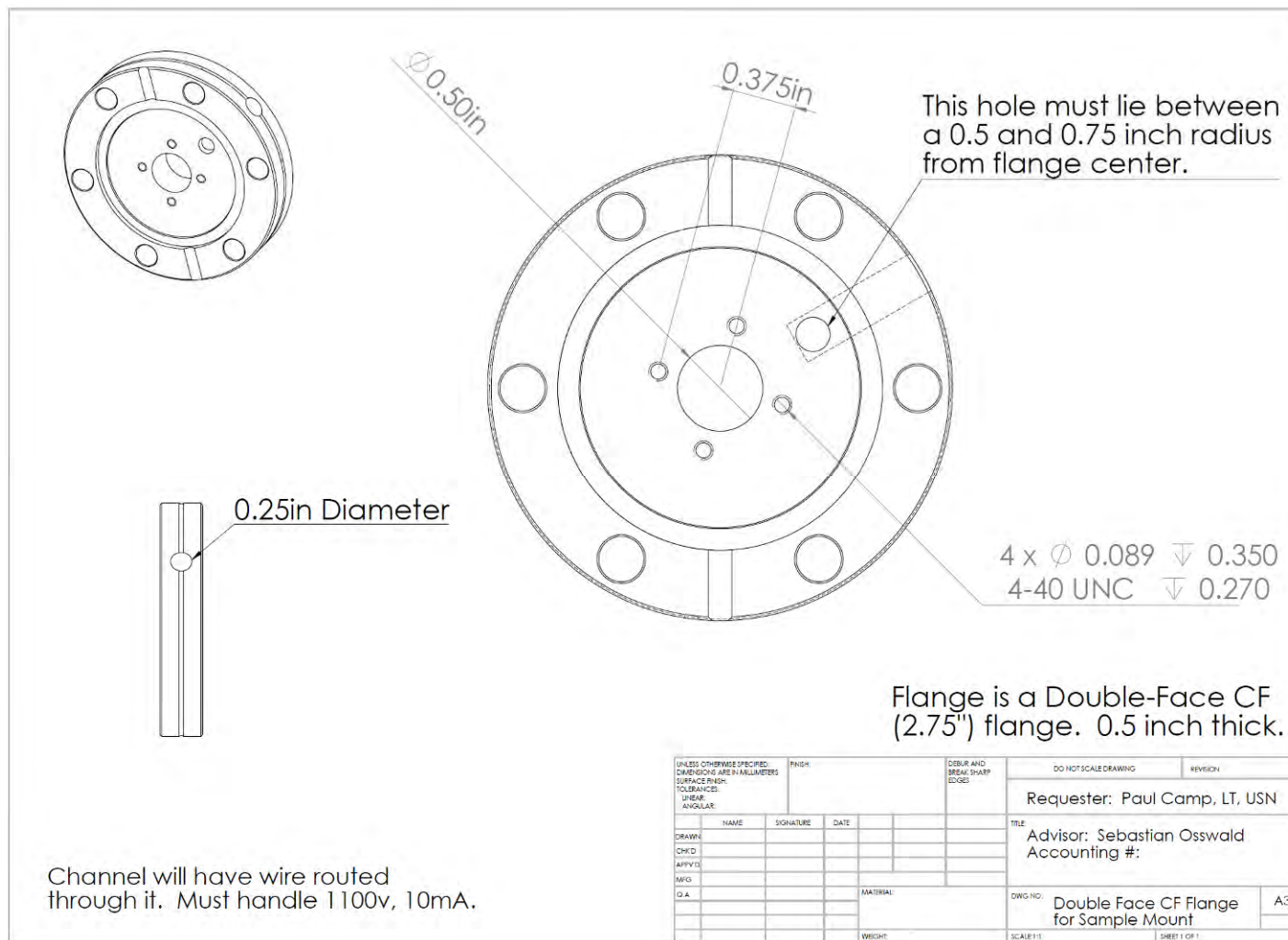


Figure 42 Sample mount

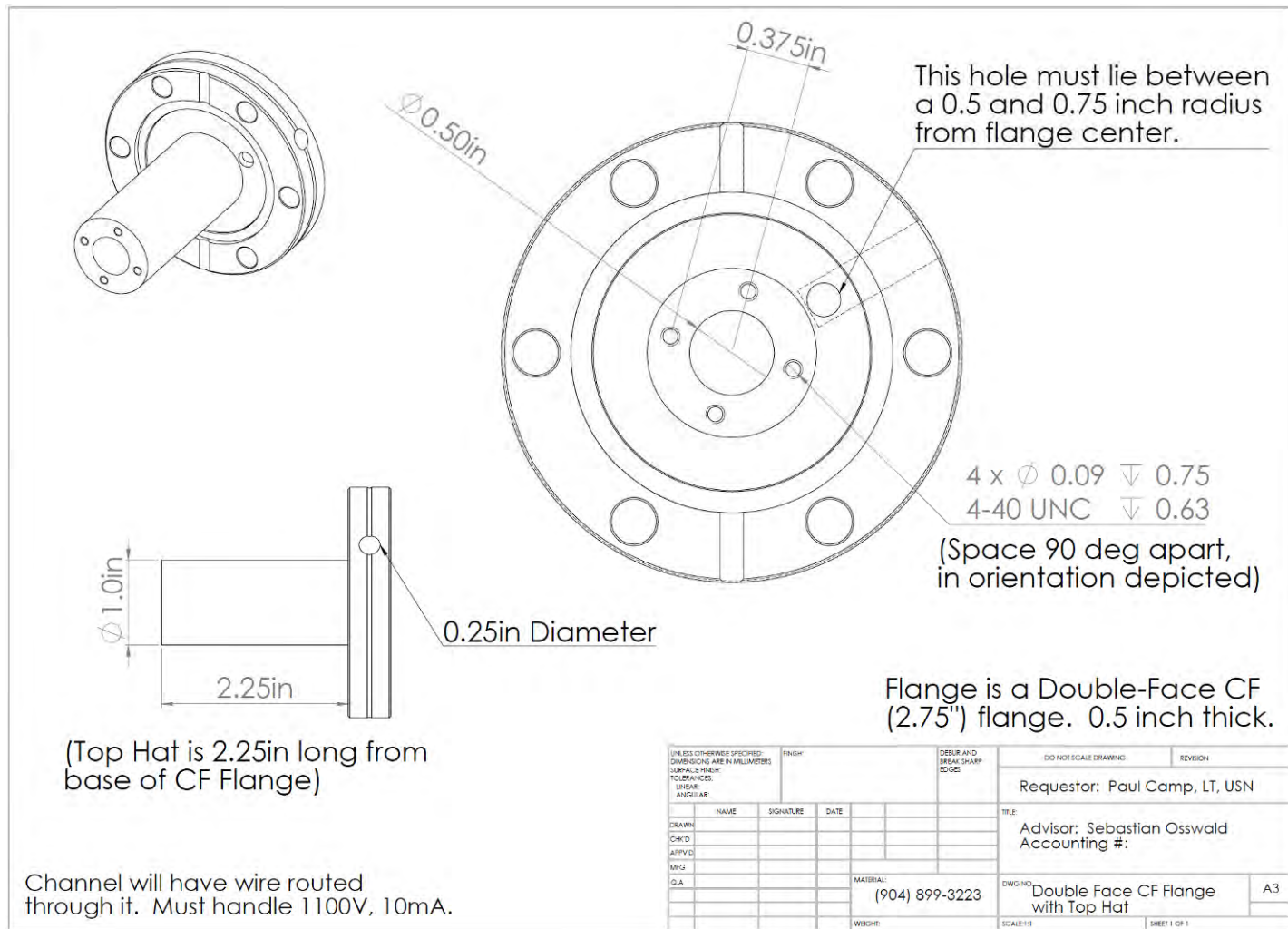


Figure 43 Top hat mount

APPENDIX B. MASS FLOW CONTROLLER OPERATING PROCEDURES

The password is set to 0000. Do not change!

The Full Scale²² of the unit is preset by the factory. Do not change! If you change the units of measurement, the Full Scale will recalculate to the units selected. If the Full Scale reads “0.000” for the units you select, this means the selected units yield a Full Scale that is beyond the resolution of the system.

POWER UP PROCEDURES

1. Confirm no gas is flowing into the MFC, and all electrical connections (CAT 5 cable, DB-15 connection, system ground) are tight and secure at both the MFC and the Pilot Module.
 - DO NOT CONNECT THE CAT 5 CABLE TO AN ETHERNET CONNECTION WHILE IT IS PLUGGED INTO THE PILOT MODULE, OR THE MFC! THIS WILL DAMAGE THE UNIT!
2. Turn power on at power strip.
 - The control valve within the MFC remains closed until power is supplied.
3. System will go through self-test. If all checks are good, Pilot Module will go to Mass Flow Rate screen.
 - Allow system to warm up for 15 minutes for optimal performance.

²² The range of measurement of the MFC.

PILOT MODULE BUTTON FUNCTIONS

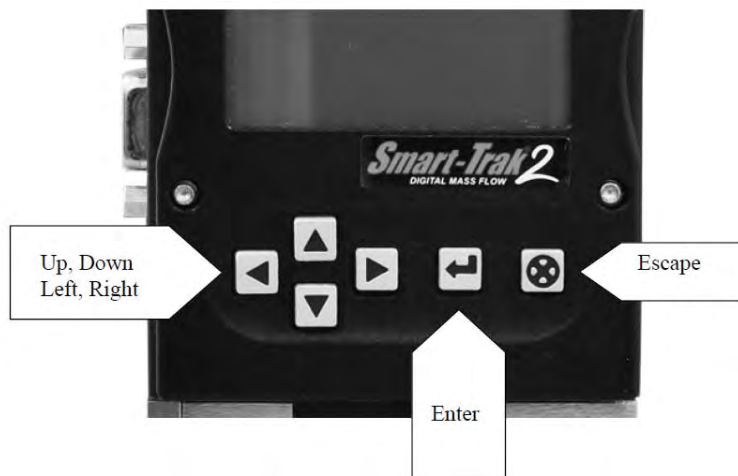


Figure 44 Pilot module buttons (From [34])

Enter – Allows the changing of a parameter; accepts the selected parameter.

Escape – Returns to Mass Flow Rate screen.

Left/Right – Select different parameters to change.

Up/Down – Change the value of the parameter.

BASIC SETUP

1. Setup Mass Flow Rate for g/hr²³ and Argon:
 - a. At the Mass Flow Rate screen, press Enter.
 - b. Enter Password, press Enter.
 - c. Press Left or Right until you reach the Change Units screen.
 - d. Press Enter to change parameter; use Up/Down to change value.
 - e. Press Enter to confirm change.
 - f. Press Right once to get to Change Gas screen.

²³ Because the Full Scale for the unit is 0–250 sccm, and the equations will use kg/sec, the units must be set to g/hr to yield a sufficient resolution to measure mass flow rate (0–24.82 grams/hr). To convert to kg/sec, divide by 3.6E6.

- g. Change gas to Argon.
- 2. Confirm Set Point Source and Value:²⁴
 - a. Press Right twice to get to Change Set Point Source.
 - b. Set source to Pilot/RS232.
 - c. Press Right until you get to Change Set Point.
 - d. Enter desired Set Point Value.

PURGING MFC

- 1. From Mass Flow Rate screen, press Enter, then press Right, until you get to the Change Valve Operation screen.
- 2. Change value to Purge.
 - The valve is now in the full open position for cleaning.
- 3. Introduce gas flow.
- 4. Allow system to purge for 1 minute.
- 5. When purging is complete, secure gas flow to MFC.
- 6. Return to the Change Valve Operation screen; change value back to Automatic.

OPERATION

- 1. Confirm no gas flow is off, and no gas flow is measured on the MFC.
- 2. Press Enter.
- 3. Enter Password, press Enter.
- 4. Cycle to Zero Meter screen.
- 5. Follow directions on screen to zero the meter.

²⁴ Set Point is the value the MFC will control the flow of gas to, i.e., enter 1.0 to control flow at 1.0 grams/hr.

6. With the MFC zeroed, the Set Point set, and Valve Operation at Automatic, introduce gas at the pressure indicated for the controller.²⁵
7. When experiment is complete, secure flow to the MFC.
8. Ensure MFC reads zero flow.
9. Secure power to the MFC.

Mass Flow Controller

| | | |
|---------------------------------|---------------|---------------------|
| Model | | |
| C100L-RD-2-OV1-SV1-PV2-V1-S0-C1 | | |
| Serial | Order | Mfg. Date |
| 146212 | 125235 | May 11, 2011 |
| Gas | | |
| ARGON | | |
| Range & Units | | STP |
| 0-250 SCCM | | 70°F / 1 ATM |
| Output Signal | | Set Signal |
| 0-5 VDC / 4-20 mA | | PILOT MODULE |
| Orientation | | Supply |
| HORIZONTAL | | 24 VDC |
| Inlet Press. | Outlet Press. | Max. Press. |
| 50 +/- 5 PSI g | 49 PSI g | 500 PSI g |
| Oper. Temp. | Max. Temp. | Connections |
| 60-70°F | 122°F | 1/4" COMP |
| O-Ring | | Valve Seat |
| Viton | | Viton |
| Technician | Cal. Date | Recal. Date |
| F.T. | May 11, 2011 | May 11, 2012 |

NOT CLEANED FOR OXYGEN SERVICE

See Instruction Manual

www.sierrainstruments.com

Made in the USA

Figure 45 MFC parameters/specifications (located on back of MFC)

²⁵ This controller has a required input pressure of 50 +/- 5 psi.

APPENDIX C. HIGH-VOLTAGE SOURCE-MEASURE UNIT OPERATING PROCEDURES

The unit requires a warm-up time of at least 1 hour to achieve rated accuracy.

WHEN OPERATE IS PRESSED/ILLUMINATED, THE UNIT IS CAPABLE OF GENERATING LETHAL VOLTAGES! EXERCISE CAUTION WHEN MANIPULATING VOLTAGE SOURCE LEADS!

Values can be entered either by the keypad on the front panel, or via < > buttons below the rotary knob, then adjust via the rotary knob.

The Green Lead provides the primary source (positive for these experiments).

DC VOLTAGE OPERATION

This operation is used when you require a constant voltage source. This will be used when the zero position for the gap distance is being determined, and when the mass flow rate and gap distance are being optimized. This is conducted strictly from the front panel of the HVSMU, with no communication from/with LabView.

1. Turn power on. Unit will commence self-test and display firmware version and IEEE address.
2. Select V – I for Source Measure switch.
3. Select DC for Function.

To determine zero gap distance

1. Set Compliance (via Compliance) to 1 microamp.²⁶
2. Set applied voltage to 1100 V.
3. Ensure system is under vacuum, with no gas flow.

²⁶ Compliance limits the maximum current generated.

4. Attach positive potential to accelerator grid, and negative potential to sample.
6. Press Operate to apply power to the apparatus.
5. Move the LSM until the sample shorts against the accelerator grid.
 - This is the point at which current is generated.
7. Note the distance displayed on the LSM position monitor program.
8. Secure power to the apparatus.
9. Move the LSM to the desired gap distance.

SWEEP VOLTAGE OPERATION

This operation is used to determine the voltages at which FE and FI occur. It will also be used during tests to characterize the performance of the CNTs. These voltages are those at which current is generated.

1. Attach positive potential to sample, and negative potential to accelerator grid.
2. Open GPIB Configuration Utility (Figure 46).

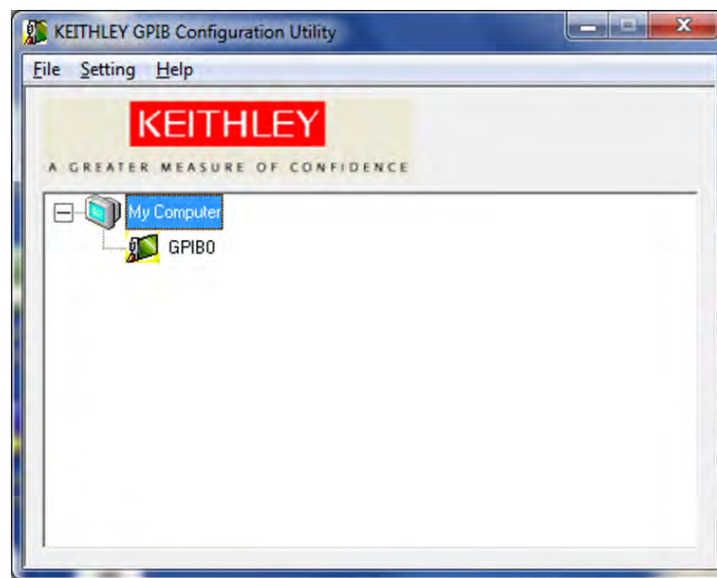


Figure 46 GPIB configuration utility

3. Double click on GPIB0 under My Computer.
4. Ensure GPIB Primary Address matches IEEE Address in HVSMU (currently set to 7).
 - The IEEE Address of the HVSMU appears during start up of the HVSMU.
5. Click Okay.
 - The TLK light on the HVSMU front panel should illuminate, if the communications connection is good.
6. Open LabView.
7. Open file: 23x Linear Stair SweepVI-repeat.vi. The Graphical User Interface (GUI) pictured below will load (Figure 47):

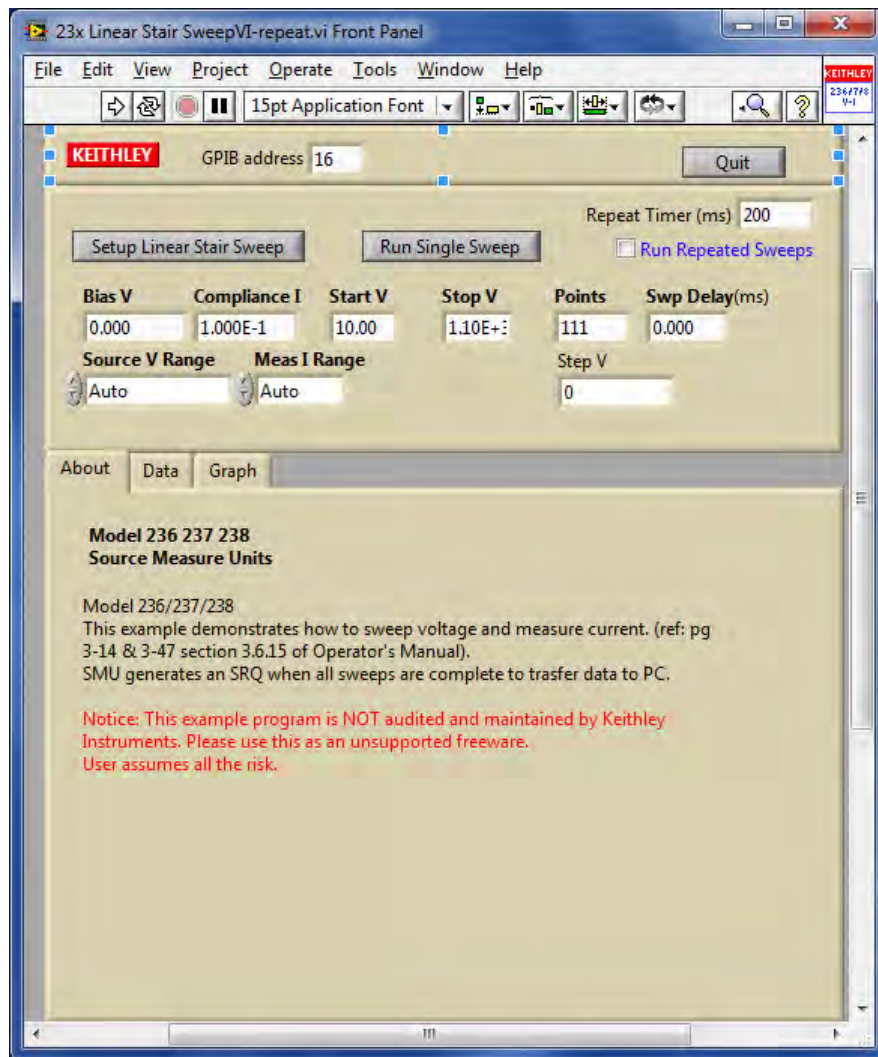




Figure 47 LabView GUI for HVSMU

8. Change GPIB address at top of GUI to that of the IEEE Address in the HVSMU.
9. Activate the GUI by clicking on the  button; the RMT and LSN lights on the HVSMU panel will illuminate. This indicates the unit is being controlled remotely from the computer.
10. Setup parameters:
 - a. Set Bias to 0 V

- b. Set Compliance, Start and Stop Voltages, and the number of data Points to desired values.
 - c. LabView will automatically calculate the necessary Step Size, based on the inputted values.
11. Click “Setup Linear Stair Sweep” button. This will setup the sweep in the HVSMU. The Trigger light will flash on the front panel, indicating the HVSMU is ready.
 12. Click “Run Single Sweep” button. This runs the inputted sweep. The TLK light will illuminate temporarily while it sends V-I data to the computer.
 13. To output the data to a .txt file for analysis, under the Data tab, click the Log switch. This will make it turn Green and say Yes. Change the file path to the desired location.
 14. When experiments are complete, click the  button, or Quit. This will disable the GUI.
 15. Close LabView and the GPIB Configuration Utility. RMT light will extinguish. Front panel operation will be restored.

THIS PAGE INTENTIONALLY LEFT BLANK

APPENDIX D. APPARATUS PARTS LIST

| Company | Part Description | Quantity | Part # |
|----------------|---|----------|----------------------|
| Kurt J. Lesker | 4-Way Cross KF40 | 2 | QF40-150-X |
| | Blank KF40 Flange | 3 | QF40-150-SB |
| | KF 40 Bellows (48" Long; Standard Unbraided Wall) | 1 | MH-QF-C48 |
| | KF 40 Bellows (24" Long; Standard Unbraided Wall) | 1 | MH-QF-C24 |
| | 2.75" CF to KF40 | | |
| | Adaptor Nipple | 2 | F0275XQF40 |
| | KF40 Tee | 1 | QF40-150-T |
| | KF40 Cast Clamp | 15 | QF40-150-C |
| | KF40 Centering Rings (SS & F/C) | 15 | QF40-150-SRV |
| | Copper Crush Gaskets (2.75") - Package of 10 | 1 | GA-0275LB (1.53" ID) |
| | Double-Faced CF | | |
| | Flange (2.75"), Blank | 2 | DFF275X000 |
| | KF40 Gate Valve | 1 | SG0150MVQF |
| | 50mm Stroke, 38mm bore, Stainless Steel Bellows | 1 | LSM38-BA-50 |
| | CF Viton Gasket (molded) - Package of 2 | 5 | VZVIT38 |
| | 1/4" OD SS Tubing - 304L (per inch) | 12 | SST-0025I |
| | KF40 90 Deg Elbow | 2 | QF40-150-E90 |
| | Linear Shift w/ | | |
| | Linear Potentiometer | 1 | LSM38-50-SS-LP-UP |
| | Sim-Step Controller | 1 | MSMC-7854-001 |
| | 5m Motor Cable | 1 | MSMC-MC |
| | Limit & Datum Cable | 1 | MSMC-LDC-UP |
| | 5m Encoder Cable | 1 | MSMC-ENC |

Table 1. Apparatus parts list

| Company | Part Description | Quantity | Part # |
|--------------------------|---|----------|-------------------------------------|
| MDC Vacuum | KF40 to Quick Connect - 1/4" | 3 | K150XDS-25 |
| Sierra Instruments | Mass Flow Controller - 100L Series | 1 | C100L-RD-2-OV1- SV1-PV2-V1-S0-C1 |
| Keithley Instruments | High-Voltage Source-Measure Unit | 1 | 237 |
| Master Pneumatic | Miniature Filter 1/4"- NPTF Fittings; 5 um filter; manual drain | 1 | F50-2T |
| | Miniature Filter Mounting Bracket | 1 | K50-01 |
| Ideal Vacuum Products | Varian Torr Seal Vacuum Equipment High Vacuum Epoxy | 1 | P102144 |

Table 2. Apparatus parts list (continued)

LIST OF REFERENCES

- [1] D. Darling, "Satellite mass categories," July 2011, http://www.daviddarling.info/encyclopedia/S/satellite_mass_categories.html.
- [2] T. M. Randolph and J. E. Polk, Jr., "An overview of the nuclear electric xenon ion system (NEXIS) activity," presented at Joint Propulsion Conference, Fort Lauderdale, FL, 2004.
- [3] C. de Coulumb, "First memoir on electricity and magnetism," *History of the Royal Academy of Sciences*, pp. 569–577, 1785.
- [4] G. P. Sutton and O. Biblarz, *Rocket Propulsion Elements* (8th ed.). Hoboken, NJ: John Wiley & Sons, 2010.
- [5] D. Darling, "NSTAR," *the encyclopedia of science: Advance propulsion concepts*, <http://www.daviddarling.info/encyclopedia/N/NSTAR.html>. Accessed November 7, 2011.
- [6] D. M. Goebel and I. Katz, *Fundamentals of Electric Propulsion: Ion and Hall Thrusters*. Hoboken, NJ: John Wiley and Sons, 2008.
- [7] C. Marrese-Reading, *et al.*, "In-FEEP thruster ion beam neutralization with thermionic and field emission cathodes," presented at 27th International Electric Propulsion Conference, Pasadena, California, 2001.
- [8] Alta SpA, "FEEP – field emission electric propulsion," *Alta-Space*, <http://www.alta-space.com/index.php?page=fEEP>. Accessed: October 24, 2011.
- [9] L. David, "CubeSats: Tiny spacecraft, huge payoff," article post to Space.COM, <http://www.space.com/308-cubesats-tiny-spacecraft-huge-payoffs.html>, September 8, 2004.
- [10] K. A. Polzin, Y. Raitses, J. C. Gayoso, and N. J. Fisch, "Comparisons in performance of electromagnet and permanent-magnet cylindrical hall-effect thrusters," presented at the 46th AIAA/ASME/SAE/ASEE Joint Propulsion Conference & Exhibit.
- [11] O. Biblarz, "AE3851: Spacecraft propulsion class notes," Naval Postgraduate School, Academic Year 2010.
- [12] R. Gomer, *Field Emission and Field Ionization* (2nd ed.). New York: American Institute of Physics, 1993.

- [13] E. Nasser, *Fundamentals of Gaseous Ionization and Plasma Electronics*. New York: John Wiley & Sons, 1971.
- [14] R. H. Fowler and L. Nordheim, "Electron emission in intense electric fields," *Proceedings of the Royal Society of London. Series A, Containing Papers of a Mathematical and Physical Character*, vol. 119, no. 781, pp. 173–181, May 1928.
- [15] T. E. Stern, B. S. Gossling, and R. H. Fowler, "Further studies in the emission of electrons from cold metals," *Proceedings of the Royal Society of London. Series A, Containing Papers of a Mathematical and Physical Character*, vol. 124, no. 795, pp. 699–723, July 1929.
- [16] R. B. Doak, "The Assessment of field ionization detectors for molecular beam use," *Journal of Physics: Condensed Matter*, vol. 16, no. 29, pp. S2863-S2878, July 2004.
- [17] Wang, X., *et al.*, "Fabrication of ultralong and electrically uniform single-walled carbon nanotubes on clean substrates," *Nano Letters*, vol. 9, no. 9, pp. 3137–3141, August 2009.
- [18] "Carbon nanotube," In *Wikipedia, The Free Encyclopedia*, http://en.wikipedia.org/wiki/Carbon_nanotube. Accessed: October 24, 2011.
- [19] T. Hicks, "A Carbon nanotube pillar array ionizer for miniature ion engine applications," M.S. thesis, Naval Postgraduate School, Monterey, California, 2008.
- [20] D. Kopeliovich, "Carbon steel SAE 1090," *SubsTech Substances & Technologies*, http://www.substech.com/dokuwiki/doku.php?id=carbon_steel_sae_1090, May 16, 2008.
- [21] Y. Min-Feng, O. Lourie, M. J. Dyer, K. Moloni, T. F. Kelly, and R. S. Ruoff, "Strength and breaking mechanism of multiwalled carbon nanotubes under tensile load," *Science*, vol. 287, no. 5453, pp. 637–640, January 2000.
- [22] S. Hong and S. Myung, "Nanotube Electronics: A flexible approach to mobility," *Nature Nanotechnology*, vol. 2, no. 4, pp. 207–207, April 2007.
- [23] E. Pop, D. Mann, Q. Wang, K. Goodson, and H. Dai, "Thermal conductance of an individual single-wall carbon nanotube above room temperature," *Nano Letters*, vol. 6, no. 1, pp. 96–100, January 2006.
- [24] "Thermal conductivity of some common materials and gases," *The Engineering Toolbox*, http://www.engineeringtoolbox.com/thermal-conductivity-d_429.html. Accessed: November 7, 2011.

- [25] M. Meyyappan, *Carbon Nanotubes*. Boca Raton: CRC Press, 2005.
- [26] H. Manohara, R. Toda, R. H. Lin, A. Liao, and M. Mojarradi, "Carbon nanotube-based digital vacuum electronics and miniature instrumentation for space exploration," *Proceedings of SPIE*, vol. 7594, pp. 75940Q-1 – 75940Q-5, February 2010.
- [27] S. Wang, X. Calderon, R. Peng, E. C. Schreiber, O. Zhou, and S. Chang, "A carbon nanotube field emission multipixel X-ray array source for microradiotherapy application," *Applied Physics Letters*, vol. 98, no. 21, pp. 213701–1 – 213701–3, May 2011.
- [28] B. P. Shrank, "Development and testing of a field ionized ion thruster for microsatellite applications," M.S. thesis, Naval Postgraduate School, Monterey, California, 2010.
- [29] O. D. Sparkman, *Mass Spectrometry Desk Reference*. Pittsburgh: Global View Publications, 2000.
- [30] B. Grüner et al., "Integrated atom detector based on field ionization near carbon nanotubes," *Physical Review*, vol. 80, no. 6, 063422–1 – 063422–7.
- [31] W. J. Ready and M. L. R. Walker, II, "Cold cathodes and ion thrusters and methods of making and using same," U.S. Patent Application 2011/0005191, January 13, 2011.
- [32] J. W. Dally, W. F. Riley, and K. G. McConnell, *Instrumentation for Engineering Measurements* (1st ed.). New York: John Wiley and Sons, Inc., 1984.
- [33] J. D. Anderson, Jr., *Hypersonic and High Temperature Gas Dynamics*. New York: McGraw-Hill, Inc., 1989.
- [34] Sierra Instruments Technical Staff, *Smart-Trak 2 Series 100 Mass Flow Meters and Controllers: Instruction Manual*, Sierra Instruments, 2011.
- [35] A. Wold, "Carbon nanotube electrode development for ion thruster miniaturization," M.S. thesis, Naval Postgraduate School, Monterey, California, 2011.

THIS PAGE INTENTIONALLY LEFT BLANK

INITIAL DISTRIBUTION LIST

1. Defense Technical Information Center
Ft. Belvoir, Virginia
2. Dudley Knox Library
Naval Postgraduate School
Monterey, California
3. Professor Sebastian Osswald
Department of Physics
Naval Postgraduate School
Monterey, California
4. Professor Marcello Romano
Department of Mechanical and Aerospace Engineering
Naval Postgraduate School
Monterey, California
5. Professor Oscar Biblarz
Department of Mechanical and Aerospace Engineering
Naval Postgraduate School
Monterey, California
6. Professor Dragoslav Grbovic
Department of Physics
Naval Postgraduate School
Monterey, California
7. Professor James Newman
Space Systems Academic Group
Naval Postgraduate School
Monterey, California
8. Professor John Lewellen
Department of Physics
Naval Postgraduate School
Monterey, California